ResearchGate

See discussions, stats, and author profiles for this publication at: https://www.researchgate.net/publication/283153193

NLTE Models Stellar Atmosphere

Research · October 2015

DOI: 10.13140/RG.2.1.2328.9049

CITATIONS
0

READS
1,673

1 author:

Mohamed Ibrahim Nouh
National Research Institute of Astronomy and Geophysics
126 PUBLICATIONS **438** CITATIONS

SEE PROFILE

All content following this page was uploaded by Mohamed Ibrahim Nouh on 25 October 2015.

The user has requested enhancement of the downloaded file.

NLTE MODELS STELLAR ATMOSPHERE

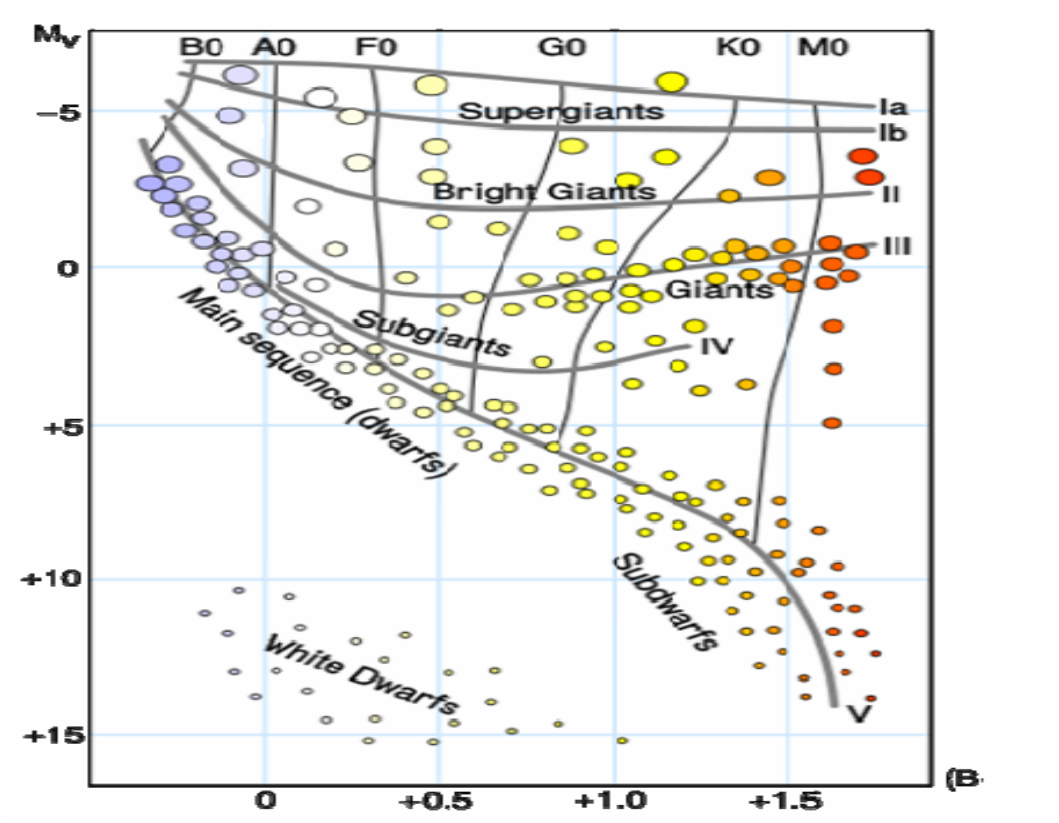

Mohamed Ibrahim Ahmed Nouh

Astronomy Department

National Research Institute of Astronomy and Geophysics

2010

Contents

List of Figures iv

1 Introduction 1

1.1 Stellar Atmospheres . . . 1

1.2 Basic Physics of Stellar Atmospheres . . . 3

1.3 State of the Art Model Atmospheres . . . 6

1.3.1 Static Models . . . 8

1.3.2 Unified Models . . . 10

2 NLTE Model Stellar Atmospheres: Numerical Methods 11

2.1 Introduction . . . 11

2.2 Basic Equations for Classical Model Atmospheres . . . 12

2.2.1 Radiation Transfer . . . 13

2.2.2 Statistical Equilibrium . . . 14

Rate Equations . . . 15

Abundance-Definition Equation . . . 16

Charge Conservation . . . 16

Complete statistical equilibrium equations . . . 17

2.2.3 Radiative Equilibrium . . . 17

2.2.4 Hydrostatic Equilibrium . . . 18

2.2.5 Particle-Conservation and Fictitious Massive-Particle Density . . . 19

2.2.6 Opacity and Emissivity . . . 20

2.2.7 Atomic Level Dissolution by Plasma Perturbations . . . 21

2.3 The Accelerated Lambda Iteration (ALI) . . . 21

2.3.1 Diagonal (Local) Lambda Operators . . . 22

2.3.2 Tridiagonal (Non-local) Lambda Operators 22
2.3.3 Acceleration of Convergence 23
2.4 Solution of the Non-linear Equations by Iteration 23
2.4.1 Discretization 23
2.4.2 Linearization 24
2.4.3 Newton-Raphson Iteration 26
2.4.4 Alternative Fast Solution Techniques for Non-linear Equations: Broyden– and Kantorovich–variants 26

3 NLTE Model Stellar Atmospheres for Different Spectral Types 28
3.1 Introduction 28
3.2 The Solar Atmosphere 30
3.3 Early Type Stars 31
3.3.1 O-type Stars 32
3.3.2 B-type Stars 35
3.3.3 A-type Stars 36
3.4 Late Type Stars 38
3.5 White Dwarfs 39
3.5.1 Helium White Dwarfs 39
3.5.2 Hydrogen White Dwarfs 40

4 Conclusion and Outlook 46
4.1 Introduction 46
4.2 Overview of the Present Theoretical Models 47
4.3 An Old-New Method: The Inversion Techniques 48
Bibliography 51

List of Figures

1.1 **Temperature structure of the solar atmosphere plotted against height, where zero is the surface (defined as where the optical depth at 500 nm reaches unity). This an idealized view to illustrate the different regions of the atmosphere. It represents the classical viewpoint from plane parallel models.** 2

1.2 **A sketch of basic atmospheric layers for early type stars.** 5

1.3 **Internal structure of C/O white dwarfs. The core of white dwarf consists of a C/O crystallized lattice (a kind of gigantic diamond), surrounded by a thick crust consisting of He and H and a small H atmosphere.** 6

3.1 **A sketch of the individual steps of astrophysical spectroscopic diagnostics of DO white dwarfs, Nouh and Fouda (2007).** 29

3.2 **Temperature structure for different models plotted against the optical depth at 500 nm.** 31

3.3 **Ionization fractions of helium and carbon in three model atmospheres, Teff = 30,000 (top), 40,000 (middle), and 50,000 K (bottom), log g = 4.0, and solar composition. LTE ionization is shown with dashed lines.** 33

3.4 **Predicted flux for three model atmospheres with (Teff, log g) equal to (40,000 K, 4.5), (35,000 K, 4.0), and (30,000 K, 4.0) (thick lines), compared to Kurucz models with the same parameters (thin histograms). Different panels show different spectrum regions.** . . 34

3.5 **Temperature structure of model atmospheres with Teff = 25,000 K, log g = 3.0 (left panel) and log g = 4.0 (right panel). Black lines show the temperature stratification of the NLTE BSTAR2006 models, compared to the LTE Kurucz models (grey lines). Solar composition models (full lines) and metal-poor (1/10 solar) models (dashed lines) are displayed. The dotted lines illustrate the effect of the different surface gravities.** 36

3.6 **Predicted flux for three solar composition model atmospheres with (Teff, log g) equal to (25,000 K, 3.0); (20,000 K, 3.0); and (15,000 K, 3.0) (black lines); compared to Kurucz (1993) models with the same parameters (grey lines).** 37

3.7 **Comparison between the observed (dots) and calculated line profiles for the O I infrared triplet. The solid line shows the NLTE calculation, and the dashed line shows the LTE profiles.** 39

3.8 **The temperature stratification for the NLTE model for DO white dwarfs at** 50000 **K,** $\log g = 8$**, He/H=** 10^2**.** 41

3.9 **The temperature stratification for the NLTE for DO white dwarfs model at** 100000 **K,** $\log g = 8$**, He/H=** 10^2**.** 41

3.10 **Line profiles computed for DO model atmospheres at different temperatures (nHe/nH = 100, log g = 7.5). NLTE is drawn with solid lines, LTE with dashed lines. The profiles are convolved with a Gaussian of 2 ÅFWHM.** 43

3.11 **Values of** T_{eff} **determined from Balmer line analyses using high metalicity non-LTE models versus the result from the pure hydrogen LTE studies.** 44

3.12 **Values of** *logg* **determined from Balmer line analyses using high metalicity non-LTE models versus the result from the pure hydrogen LTE studies.** 45

Chapter 1

Introduction

1.1 Stellar Atmospheres

Much of stellar astronomy depends upon the observation and interpretation of the electromagnetic radiation radiated by stars. The region near the surface of the star from which photons can escape directly to space without undergoing further absorption or scattering is referred to as the atmosphere. It represents the boundary between the relatively simple physics of the stellar interior, where strict thermodynamic equilibrium accurately describes the state of the material, and the surrounding vacuum of space.

The atmosphere thus represents a region of large gradients in the physical variables such as the temperature, gas pressure and the radiation field. It is also where the stellar material becomes optically thin with the result that the radiation field is no longer strongly coupled to the local environment. As such, stellar atmospheres are comparatively difficult to model. A meaningful interpretation of stellar spectra, however, is only possible with the assistance of consistent models. Consequently, much effort has been devoted to the construction of such models over the past fifty years.

The radiation that reaches us from stars is in most cases the only tool available to study them. The stellar radiation has encoded information about its formation place, the photosphere. The photosphere is typically a very small layer when compared to the stellar radius. In the Sun its length is about 1000 km (to the solar radius, this thickness has a similar proportion as the apple skin to the apple). Despite its relatively thin size, the importance of the photosphere is considerable. Most of a star's spectrum is formed in the

photosphere, making it the only region that can be extensively studied for the majority of stars. A simplified view of the structure of the solar atmosphere, including the photosphere, is given in Figure (1.1), Pereira (2009). Throughout this review the more loosely defined term 'atmosphere' will be used to refer to the photosphere. This is because models of stellar photospheres are computed for the photosphere and surrounding regions, but usually do not include the chromosphere or other higher regions. Yet they are called models of stellar atmospheres, although they are constructed to study the photospheres. It is of the utmost

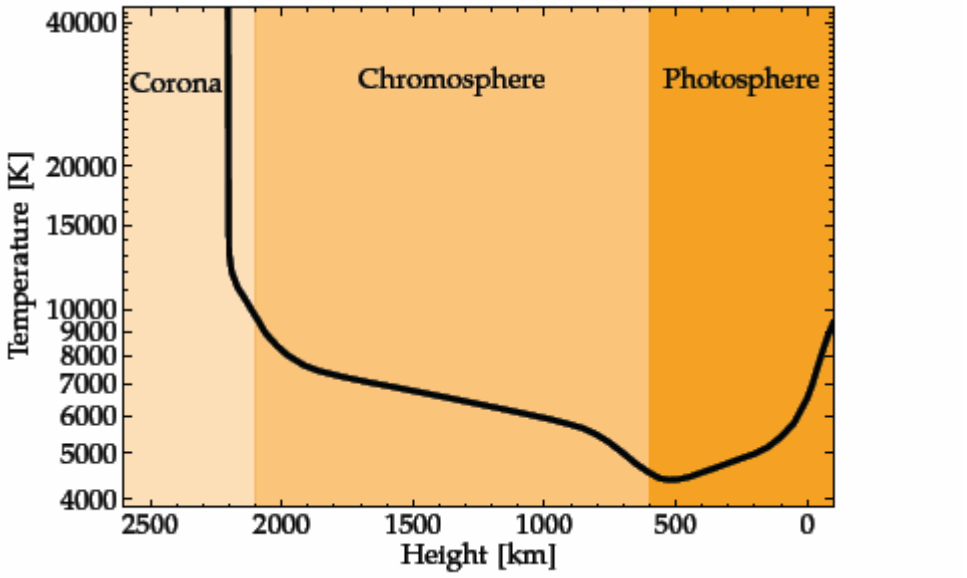

Figure 1.1: **Temperature structure of the solar atmosphere plotted against height, where zero is the surface (defined as where the optical depth at 500 nm reaches unity). This an idealized view to illustrate the different regions of the atmosphere. It represents the classical viewpoint from plane parallel models.**

importance to understand the physical processes that take place in the photosphere so that information about the star can be inferred. Quantities like effective temperature, gravity, radius, rotation and chemical composition can be obtained by studying stellar photospheres.

The most interesting property that can be obtained through the study of photospheres

and spectra is arguably the chemical composition of stars. The chemical composition traces the history of the Universe, Pereira (2009). It allows astronomers and cosmologists to trace the origin and evolution of elements, which ultimately provides insight in a multitude of disciplines. Its study can provide the answers to questions like how did the Big Bang create heavy elements, how galaxies form and evolve, which stellar systems have the conditions to host life, etc.

1.2 Basic Physics of Stellar Atmospheres

From the physical point of view, a stellar atmosphere is generally a plasma composed of many kinds of particles, namely atoms, ions, free electrons, molecules, or even dust grains. In hot stellar atmosphere, because of the high temperature and strong radiation field, there are typically no molecules nor dust grains present, at least in the layers that are traditionally considered as an atmosphere. Nevertheless, molecules and dust may still be present in the very remote parts of an atmosphere.

The total particle density in the stellar atmosphere ranges from, say, 10^6 cm^3 (main sequence stars) to $10^{16} cm^3$ (compact stars) . It can be shown that under these densities the elastic collisions between particles are frequent enough to yield very nearly a Maxwellian velocity distribution for all particles; moreover with the same associated kinetic temperature. It should be stressed that this temperature is shared only by massive particles; massless particles, like photons, do not generally possess an equilibrium distribution and thus a corresponding temperature.

The other critical feature that follows from the presence of radiation-induced processes is that the medium is prone to departures from thermodynamic equilibrium. Indeed, the simple fact that we do see a star means that photons must escape from the atmosphere (in fact, this is a very definition of an atmosphere). Hence the photons must be missing in the atmosphere, and thus some elementary atomic transition processes can no longer be balanced, which leads to a non-equilibrium situation.

The physical processes occur throughout the atmosphere are different when one go from spectral type to another. Here, it is sufficient to mention only three spectral regions

through the HR diagram, namely, early-type stars, late type-stars and compact stars (here we namely describe white dwarf atmospheres only).

- **Early Type Stars:** The atmospheres of early-type stars is mainly characterized by strong and energetic radiation field generated in their interiors, the radiation in their atmospheres is not merely a passive probe of the physical state of the atmosphere, but rather an important energy balance agent. In other words, radiation in fact determines the structure of the medium, yet the medium is probed only by this radiation. **Another important feature is that photons have, under the conditions met in the early-type stellar atmospheres, a much larger mean-free-path than massive particles. This means that radiation is able to transport information to large distances; in other words, radiation couples the physical states of rather distant regions of the atmosphere, Mihalas(1978)**. A sketch of basic atmospheric layers for early type stars is shown in Figure (1.2).

- **Late Type Stars:** The atmosphere of the late type stars is so different from that of early type stars in many situations. Due to the low temperature of the late type stars, the radiation does not play the main role in energy transfer, the convection is very important in these stars. Molecular spectra which is nearly disappeared in early type stars, is clearly seen in the spectra of late type stars and is a fundamental tool for the spectral diagnostic of these stars.

- **White Dwarfs:** Although most white dwarfs are thought to be composed of carbon and oxygen, spectroscopy typically shows that their emitted light comes from an atmosphere which is observed to be either hydrogen-dominated or helium-dominated. The dominant element is usually at least 1,000 times more abundant than all other elements. As explained by Schatzman in the 1940s, the high surface gravity is thought to cause this purity by gravitationally separating the atmosphere so that heavy elements are on the bottom and lighter ones on top. This atmosphere, the only part of the white dwarf visible to us, is thought to be the top of an envelope which is a residue of the star's envelope in the AGB phase and may also contain material accreted from

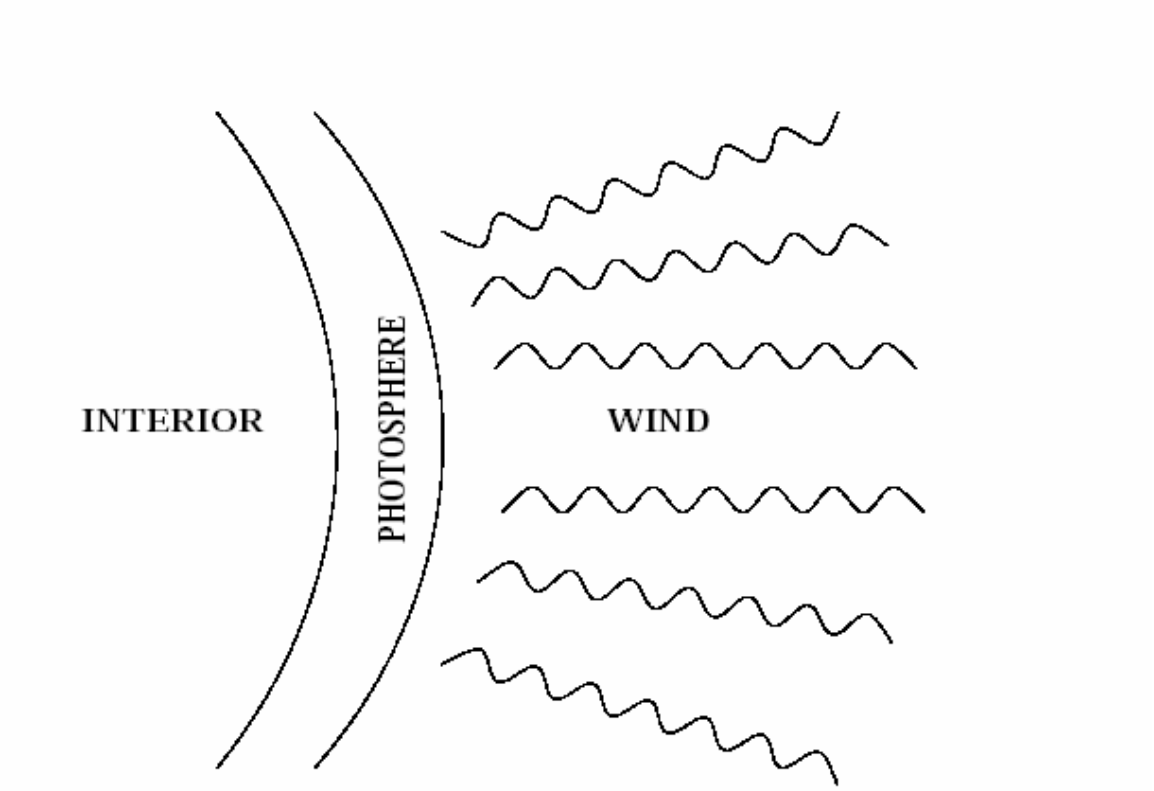

Figure 1.2: **A sketch of basic atmospheric layers for early type stars.**

the interstellar medium. The envelope is believed to consist of a helium-rich layer with mass no more than 1/100th of the star's total mass, which, if the atmosphere is hydrogen-dominated, is overlain by a hydrogen-rich layer with mass approximately 1/10,000th of the stars total mass.

To say that white dwarfs are strange is an understatement. An earth–sized white dwarf has a density of 1×10^9 kg/m^3 . In comparison, the earth itself has an average density of only 5.4×10^3 kg/m^3 . That means a white dwarf is 1 million times as dense.

Underneath the atmosphere, scientists believe there is a 50 km thick crust, the bottom

of which is a crystalline lattice of carbon and oxygen atoms. One might make the comparison between a cool carbon/oxygen white dwarf and a diamond. Typical WD structure is displayed in Figure (1.3).

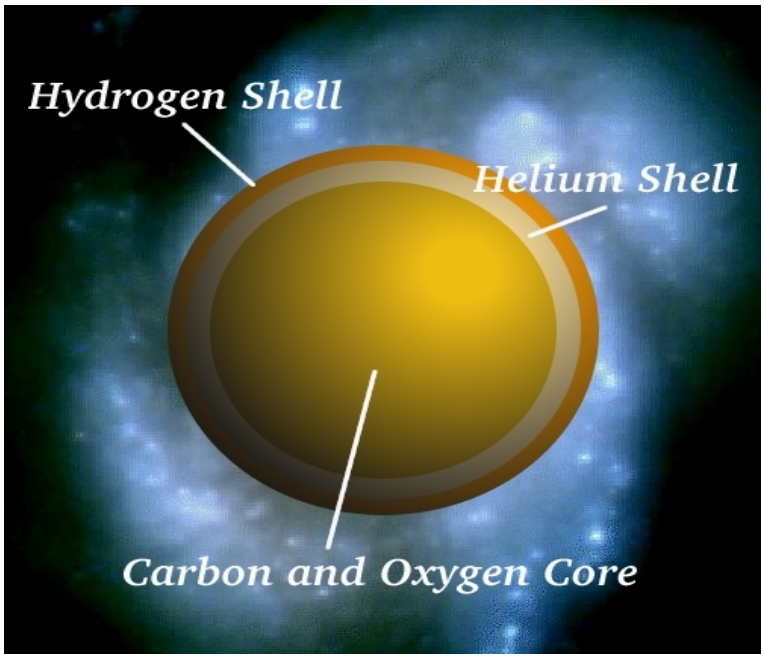

Figure 1.3: **Internal structure of C/O white dwarfs. The core of white dwarf consists of a C/O crystallized lattice (a kind of gigantic diamond), surrounded by a thick crust consisting of He and H and a small H atmosphere.**

1.3 State of the Art Model Atmospheres

By the term model atmosphere we understand a specification of all the atmospheric state parameters as functions of depth. Since the problem is very complex, we cannot construct analytic solutions. Therefore, we discretize the depth coordinate and consider a definite number of depth points, this number is typically of the order of several tens to few hundreds.

A model atmosphere is then a table of values of the state parameters in these discretize depth points.

Which are the parameters that describe the physical state of the atmosphere?. The list of parameters depend on the type of the model, i.e. on the basic assumptions under which the model is constructed. Traditionally, the list of state parameters includes only massive particle state parameters (e.g. temperature, density, etc.), but not the radiation field parameters. This might seem to be in sharp contrast of what was being stated before, namely that radiation intensity is in fact a crucial parameter. It indeed is, and in fact the radiation intensity is an important state parameter in the process of constructing the atmospheric structure. But, when the system of all structural equations, which includes the radiative transfer equation, is solved, we do not have to keep the radiation intensity in the list of state parameters which has to be stored in the table representing the model. The point is that once all the necessary material properties are given, we may easily determine the radiation field by a formal solution of the transfer equation.

State of the art NLTE model atmospheres provide realistic synthetic spectra which are in the case of hot stars indispensable for precise analyses of photospheric properties as well as for analyses of e.g. planetary nebulae where it is highly recommended to use metalline blanketed NLTE model atmosphere fluxes as ionizing spectra. For cool stars with spectral type B or later in many cases fully lineblanketed LTE model atmospheres (Kurucz 1979, 1991) are commonly used in order to determine photospheric parameters – but there are always NLTE effects in any star and reliable NLTE models can be essential. **Thus, the use of NLTE model atmospheres is recommended – not only for hot stars**.

Unfortunately, the calculation of NLTE models is much more complicated: An extremely nonlinear system of statistical equilibrium equations and radiation transfer equations has to be solved simultaneously! Pioneering work was presented by Auer & Mihalas (1969, complete linearization, CL). Based on their method, Auer & Mihalas (1972) and Kudritzki (1976) calculated H+He models (lowest five H i levels treated in NLTE + six line transitions, 65 frequency points). A first attempt to consider metal opacities was done by Mihalas (1972) who introduced an "average light element" in addition to H and He. Hus-

feld (1984) considered the light elements H+He+C+N+O (ground states of CNO treated in NLTE) in more detail. However, although this method had proved to be very stable, the numerical limitation of this approach was severe prohibiting adequate analyses of the available spectra at that time.

A huge step forward was done by Werner (1986) who calculated the first model atmospheres based on the newly developed Accelerated Lambda Iteration ("ALI") method. The separation of statistical equations and radiative equations made it possible to take metalline blanketing into account. Anderson (1990) presented NLTE calculations with millions of lines of the elements HFe (MultiFrequency/MultiGray algorithm). Detailed calculations of H+He+C+N+O models (up to a total of more than 200 levels treated in NLTE, 1 000 line transitions, 10 000 frequency points) were performed e.g. by Dreizler & Werner (1991) and Rauch & Werner (1991). A hybrid CL/ALI method (Hubeny & Lanz 1993, 1995) was used for the detailed studies on the impact of irongroup elements. Present state of the art models (Dreizler & Werner 1993, Rauch 1993, 1997) include all elements from hydrogen to the iron group and the opacities of millions of irongroup lines.

In the following subsections, we will discuss the types of model stellar atmospheres constructed under certain physical and geometrical conditions.

1.3.1 Static Models

These are models constructed under the assumption of hydrostatic equilibrium. Consequently, these models apply only to atmospheric layers that are indeed close to hydrostatic equilibrium, i.e. the macroscopic velocity is small compared to the thermal velocity of atoms. Basic input parameters are the effective temperature, the surface gravity, g (usually expressed Te., as log g), and chemical composition. Strictly speaking, one should give the values of abundances of all individual chemical species. In reality, one usually considers solar abundances, or some ratio of some or all abundances with respect to the solar one. If all elements but hydrogen and helium share the common abundance ratio with respect to the solar abundances, this ratio is called metallicity. There are some additional input parameters, like the microturbulent velocity, or, in the case of convective models, the mixing

length (or some other parameters approximating the convection). There are several basic types of models:

- LTE grey models. They are the simplest possible models, based on the assumption that the opacity is independent of frequency. They are not used any longer for spectroscopic work, but they are useful for providing an initial estimate in any iterative method for constructing more realistic models, and they are very useful for pedagogical purposes.

- LTE models. They are based on the assumption of LTE. Two state parameters, for instance temperature,T , and density, (or electron density, ne), suffice to describe the physical state of the atmosphere at any given depth.

- NLTE models. This is a rather ambiguous term which encompasses any model which takes into account some kind of a departure from LTE. In early NLTE models, the populations of only few of the low-lying energy levels of the most abundant species, like H and He, were allowed to depart from LTE; the rest was treated in LTE. There are two basic kinds of NLTE models, or approaches to include NLTE effects:

  - Models solving for the full structure. The codes of general use include an early H-He model atmosphere code described by Mihalas et al. (1975), the Kiel code (Werner 1987); PAM (Anderson 1987), and a universal code TLUSTY (Hubeny 1988).

  - NLTE line formation (also called a restricted NLTE problem). Here, the atmospheric structure (temperature, density, etc.) is assumed to be known form previous calculations (either LTE or simplified NLTE), and is kept fixed, while only radiative transfer and statistical equilibrium for a chosen atom/ion is solved simultaneously.

  - NLTE line-blanketed models. This is in fact a subset of the previous item. One considers it separately because these models represent a qualitatively new step in the model construction. They are models where NLTE is considered for

practically all energy levels and transitions between them lines and continua that influence the atmospheric structure. The number of such lines may actually go to millions, so the problem is presently extremely demanding on the computer resources and powerful of the numerical methods used. In these models, it is no longer necessary to compute the atmospheric structure using simple atomic models, and recalculate NLTE line formation in individual atoms separately.

1.3.2 Unified Models

By definition, unified model atmosphere are those which relax the a priori assumption of hydrostatic equilibrium, and which thus treat the whole atmosphere ranging from an essentially static photosphere to a highly dynamical wind on the same footing. Ideally, this would mean solving self-consistently the set of hydrodynamic equations and the radiative transfer equation. This is a tremendous task, which has not yet been even attempted to solve generally. Instead, one treats the hydrodynamic of the wind taking into account radiation in some approximate way (for instance, the line driven wind theory by Castor, Abbott, Klein 1975; or Pauldrach, Puls, Kudritzki 1986. Once the basic hydrodynamic structure (essentially, the density and velocity as a function of radius) is determined, NLTE radiative transfer together with the radiative equilibrium equation could be solved in details. This approach was pioneered by the Munich group (Gabler et al. 1989; Sellmaier et al. 1993), who also coined the term "unified models". The name stresses a unification of a photosphere and wind; prior to this approach there were separate models for photospheres and for winds, so-called core-halo models.

Chapter 2

NLTE Model Stellar Atmospheres: Numerical Methods

2.1 Introduction

The first pioneering work on NLTE was presented by Auer & Mihalas (1969, complete linearization, CL). Based on their method, Auer & Mihalas (1972) and Kudritzki (1976) calculated H+He models (lowest five H i levels treated in NLTE + six line transitions, 65 frequency points).

A first attempt to consider metal opacities was done by Mihalas (1972) who introduced an "average light element" in addition to H and He. Husfeld (1984) considered the light elements H+He+C+N+O (ground states of CNO treated in NLTE) in more detail. However, although this method had proved to be very stable, the numerical limitation of this approach was severe preventing adequate analyses of the available spectra at that time.

A hybrid CL/ALI method (Hubeny & Lanz 1993, 1995) was used for the detailed studies on the impact of iron group elements. Present state of the art models (Dreizler & Werner 1993, Rauch 1993, 1997) include all elements from hydrogen to the iron group and the opacities of millions of iron group lines.

In the next chapter, numerical methods commonly implemented to solve the classical model atmosphere problem will be outlined.

2.2 Basic Equations for Classical Model Atmospheres

The classical model atmospheres assume plane-parallel geometry, which is well justified for most stars because the atmospheres are thin compared to the stellar radius. The only parameters needed to characterize uniquely such an atmosphere are the effective temperature ($T_{\rm eff}$), a measure for the amount of energy transported through the atmosphere per unit area and time, the surface gravity (g), and the chemical composition.

To construct model atmospheres we must solve simultaneously a set of equations that is highly coupled and non-linear. Because of the coupling, no equation determines uniquely a single quantity – *all* equations jointly determine each of the state parameters. Neverlethess, each of them is usually thought of as determining, more or less, a particular quantity. These equations are:

- The radiation transfer equations which are solved for the angle-integrated mean intensities $J_i, i = 1, \ldots, NF$, on a pre-chosen frequency grid comprising NF points. The formal solution is given by $J = \Lambda S$, where S is the source function, and Λ is the transport operator. Although Λ is written as an operator, one may think of it as a *process* of obtaining the mean intensity from the source function.

- The hydrostatic-equilibrium equation which determines the total particle density N.

- The radiative-equilibrium equation from which the temperature T follows.

- The particle-conservation equation, determining the electron density n_e.

- The statistical-equilibrium equations, which are solved for the population densities $n_i, i = 1, \ldots, NL$ of the atomic levels that are allowed to depart from LTE (NLTE levels).

- The equation that defines a fictitious massive-particle density n_H, which is introduced for convenience in the solution procedure.

2.2.1 Radiation Transfer

Any numerical method requires a formal solution (i.e. atmospheric structure already given) of the radiation transfer problem. Radiation transfer at any depth point is described by the transfer equation:

$$\pm\mu\frac{\partial I_\nu(\pm\mu)}{\partial\tau_\nu} = S_\nu - I_\nu(\pm\mu), \quad \mu\in[0,1], \tag{2.1}$$

written separately for positive and negative μ (the angle-cosine between the direction of propagation and the outward-directed normal to the surface), i.e. for the inward and outward directional intensities $I(\mu)$ at frequency ν. Here τ_ν is the optical depth (defined in terms of the column mass m used in the other structural equations by $d\tau_\nu = dm\chi_\nu/\rho$, where ρ is the mass density), and S_ν is the local source function. Introducing the Feautrier intensity

$$u_{\nu\mu} \equiv \left(I_\nu(\mu) + I_\nu(-\mu)\right)/2 \tag{2.2}$$

we obtain the second-order form (Mihalas 1978, p. 151):

$$\mu^2\frac{\partial^2 u_{\nu\mu}}{\partial\tau_\nu^2} = u_{\nu\mu} - S_\nu, \quad \mu\in[0,1]. \tag{2.3}$$

We may separate the Thomson emissivity term (scattering from free electrons, assumed coherent, with cross-section σ_e) from the source function so that

$$S_\nu = S'_\nu + n_e\sigma_e J_\nu/\chi_\nu, \tag{2.4}$$

where S'_ν is the ratio of thermal emissivity to total opacity as described in detail below: $S'_\nu = \eta_\nu/\chi_\nu$. The mean intensity is the angular integral over the Feautrier intensity, hence the transfer equation becomes

$$\mu^2\frac{\partial^2 u_{\nu\mu}}{\partial\tau_\nu^2} = u_{\nu\mu} - S'_\nu - \frac{n_e\sigma_e}{\chi_\nu}\int_0^1 u_{\nu\mu}\,d\mu. \tag{2.5}$$

Thomson scattering complicates the situation by its explicit angle coupling but the solution can be obtained with the standard Feautrier scheme. Assuming complete frequency-redistribution in spectral lines (Mihalas 1978, p. 29), no explicit frequency coupling occurs

so that a parallel solution for all frequencies enables very efficient vectorization on the computer.

The following boundary conditions are used for the transfer equation. At the inner boundary where the optical depth is at maximum, $\tau = \tau_{\max}$, we have

$$\left(\mu \frac{\partial u_{\nu\mu}}{\partial \tau_\nu}\right)_{\tau_{\max}} = I^+_{\nu\mu} - u_{\nu\mu}(\tau_{\max}), \tag{2.6}$$

where we specify $I^+_{\nu\mu} = I_\nu(+\mu, \tau_{\max})$ from the diffusion approximation:

$$I^+_{\nu\mu} = B_\nu + \frac{3\mu}{\chi_\nu}\frac{\partial B_\nu}{\partial T}\frac{\mathcal{H}}{\int_0^\infty \frac{1}{\chi_\nu}\frac{\partial B_\nu}{\partial T}\, d\nu}. \tag{2.7}$$

Here B_ν is the Planck function and $\mathcal{H}$ the nominal (frequency-integrated) Eddington flux:

$$\mathcal{H} = \sigma_R T^4_{\rm eff}/4\pi, \tag{2.8}$$

with the Stefan-Boltzmann constant σ_R. At the outer boundary we take $\tau_\nu = \tau_{\min} = m_1\chi_\nu/2\rho$, assuming that χ is a linear function of m for $m < m_1$. Since $\tau_{\min} \neq 0$, it is not exactly valid to assume no incident radiation at the stellar surface. Instead we specify $I^-_{\nu\mu} = I_\nu(-\mu, \tau_{\min})$ after Scharmer & Nordlund (1982):

$$I^-_{\nu\mu} = S_\nu(\tau_{\min})[1 - \exp(-\tau_{\min}/\mu)] \tag{2.9}$$

which follows from Eq. 2.1 assuming $S(\tau) = S(\tau_{\min})$ for $\tau < \tau_{\min}$. Then we get:

$$\left(\mu \frac{\partial u_{\nu\mu}}{\partial \tau_\nu}\right)_{\tau_{\min}} = u_{\nu\mu}(\tau_{\min}) - I^-_{\nu\mu}. \tag{2.10}$$

The boundary conditions are discretized performing Taylor expansions which yield second-order accuracy (Mihalas 1978, p. 155).

2.2.2 Statistical Equilibrium

The statistical equilibrium equations are set up according to Mihalas (1978, p. 127). The number of atomic levels, ionization stages, and chemical species, as well as all radiative and collisional transitions are taken from the input model atom supplied by the user. Ionization into excited states of the next ionization stage is taken into account. Dielectronic recombination and autoionization processes can also be included in the model atom.

Rate Equations

As usual, the atomic energy levels are ordered sequentially by increasing excitation energy, starting with the lowest ionization stage. Then for each atomic level i of any ionization stage of any element, the rate equation describes the equilibrium of rates into and rates out of this level:

$$n_i \sum_{i \neq j} P_{ij} - \sum_{j \neq i} n_j P_{ji} = 0. \tag{2.11}$$

The rate coefficients P_{ij} have radiative and collisional components: $P_{ij} = R_{ij} + C_{ij}$. Radiative upward and downward rates are respectively given by:

$$R_{ij} = 4\pi \int_0^\infty \frac{\sigma_{ij}(\nu)}{h\nu} J_\nu \, d\nu, \tag{2.12}$$

$$R_{ji} = \left(\frac{n_i}{n_j}\right)^\star 4\pi \int_0^\infty \frac{\sigma_{ij}(\nu)}{h\nu} \left(\frac{2h\nu^3}{c^2} + J_\nu\right) e^{-h\nu/kT} \, d\nu. \tag{2.13}$$

Photon cross-sections are denoted by $\sigma_{ij}(\nu)$. $(n_i/n_j)^\star$ is the Boltzmann LTE population ratio in the case of line transitions: $g_i/g_j \exp(-h\nu_{ij}/kT)$, where the $g_{i,j}$ are the statistical weights. The LTE population number of a particular level is defined relative to the ground state of the next ion, so that in the case of recombination from a ground state n_1^+ we have by definition $(n_i/n_j)^\star = n_e \phi_i(T)$ with the Saha-Boltzmann factor

$$\phi_i(T) = 2.07 \cdot 10^{-16} \frac{g_i}{g_1^+} T^{-3/2} e^{h\nu_i/kT}, \tag{2.14}$$

where $h\nu_i$ is the ionization potential of the level i. Care must be taken in the case of recombination from an excited level into the next lower ion. Then $(n_i/n_j)^\star = n_e \phi_i \cdot \phi_1^+ / \phi_j$.

Dielectronic recombination is included following Mihalas & Hummer (1973). Assuming now that j is a ground state of ion k, then the recombination rate into level i of ion $k-1$ via an autoionization level c (with ionization potential $h\nu_c$, having a negative value when lying above the ionization limit) is:

$$R_{ji} = \frac{8\pi^2 e^2}{mc^3} n_e \phi_i f_{ic} e^{h(\nu_c - \nu_i)/kT} \nu_c^2 \left(1 + \frac{c^2}{2h\nu_c^3 \bar{J}}\right). \tag{2.15}$$

The reverse process, the autoionization rate, is given by:

$$R_{ij} = \frac{4\pi^2 e^2}{hmc} \frac{1}{\nu_c} f_{ic} \bar{J}. \tag{2.16}$$

The oscillator strength for the stabilizing transition (i.e. transition $i \rightarrow c$) is denoted by f_{ic}, and $\bar{J}$ is the mean intensity averaged over the line profile. Our program simply takes J_ν from the continuum frequency point closest to the transition frequency, which is reasonable because the autoionization line profiles are extremely broad. The population of autoionization levels is assumed to be in LTE and therefore such levels do not appear explicitly in the rate equations.

The computation of collisional rates is generally dependent on the specific ion or even transition. Several options, covering the most important cases, may be chosen by the user.

Abundance-Definition Equation

The rate equation for the highest level of a given chemical species is redundant. It is replaced by the abundance definition equation. Summation over all levels usually includes not only NLTE levels but also levels which are treated in LTE, according to the specification in the model atom. Denoting the number of ionization stages of species k with $NION(k)$, the number of NLTE and LTE levels per ion with $NL(l)$ and $LTE(l)$, respectively, we can write:

$$\sum_{l=1}^{NION(k)} \left[\sum_{i=1}^{NL(l)} n_{kli} + \sum_{i=1}^{LTE(l)} n^{\star}_{kli} \right] = y_k(N - n_e). \tag{2.17}$$

y_k is the number fraction of element k.

Charge Conservation

We close the system of statistical equilibrium equations by demanding charge conservation. We denote the total number of chemical species with $NATOM$, the charge of ion l with $q(l)$ (in units of the electron charge) and write:

$$\sum_{k=1}^{NATOM} \sum_{l=1}^{NION(k)} q(l) \left[\sum_{i=1}^{NL(l)} n_{kli} + \sum_{i=1}^{LTE(l)} n^{\star}_{kli} \right] = n_e. \tag{2.18}$$

Complete statistical equilibrium equations

We introduce a vector comprising the occupation numbers of all NLTE levels, $\mathbf{n} = (n_1, \ldots, n_{NL})$. Then the statistical equilibrium equation is written as:

$$\mathbf{An} = \mathbf{b}. \tag{2.19}$$

The gross structure of the rate matrix $\mathbf{A}$ is of block matrix form, because transitions between levels occur within one ionization stage or to the ground state of the next ion. The structure is complicated by ionizations into excited levels and by the abundance definition and charge conservation equations which give additional non-zero elements in the corresponding lines of $\mathbf{A}$.

2.2.3 Radiative Equilibrium

Radiative equilibrium can be enforced by adjusting the temperature stratification either during the linearization procedure or in between ALI iterations. In the former case a linear combination of two different formulations is used and in the latter case the classical Unsöld-Lucy temperature correction procedure (Lucy 1964) is utilized. The latter is particularly interesting, because it allows one to exploit the block form of the rate-coefficient matrix. This fact allows an economic block-by-block solution followed by a subsequent Unsöld-Lucy temperature correction step. On the other hand, however, this correction procedure may decelerate the global convergence behavior of the ALI iteration.

The two forms of expressing the radiative equilibrium condition follow from the requirement that the energy emitted by a volume element per unit time is equal to the absorbed energy per unit time (integral form):

$$\int_0^\infty \chi_\nu (S_\nu - J_\nu)\, d\nu = 0, \tag{2.20}$$

where scattering terms in χ_ν and S_ν cancel out. In principle, this formulation is equivalent to demanding flux-constancy throughout the atmosphere (differential form)

$$\int_0^\infty \frac{\partial}{\partial \tau_\nu}(f_\nu J_\nu)\, d\nu - \mathcal{H} = 0, \tag{2.21}$$

where $\mathcal{H}$ (Eq. 2.8) is the nominal flux. Here f_ν is the variable Eddington factor, defined as

$$f_\nu = \int_0^1 \mu^2 u_{\nu\mu}\, d\mu \Big/ \int_0^1 u_{\nu\mu}\, d\mu, \tag{2.22}$$

which is computed from the Feautrier intensity $u_{\nu\mu}$ (Eq. 2.2) after the formal solution. As discussed e.g. in Hubeny (1988) the differential form is more accurate at large depths, while the integral form behaves numerically superior at small depths. Instead of arbitrarily selecting that depth in the atmosphere where we switch from one formulation to the other, we use a linear combination of both constraint equations, which guarantees a smooth transition with depth, based on physical grounds (Hubeny & Lanz 1992):

$$\frac{1}{\bar{\kappa}_J} \int_0^\infty \chi_\nu (S_\nu - J_\nu)\, d\nu + \bar{\Lambda}^\star_J \int_0^\infty \frac{\partial}{\partial \tau_\nu}(f_\nu J_\nu)\, d\nu - \bar{\Lambda}^\star_J \mathcal{H} - F_0 = 0. \tag{2.23}$$

We note that explicit depth coupling is introduced by the differential form Eq. 2.21 through the derivative $\partial/\partial\tau_\nu$ even if a purely local $\Lambda^\star$ operator is used. Therefore the linearization procedure can no longer be performed independently at each depth point and the question at which boundary to start becomes relevant. Numerical experience shows that it is essential to start at the outer boundary and proceed inwards. If a tri-diagonal operator is used, nearest neighbor depth coupling is introduced anyhow.

2.2.4 Hydrostatic Equilibrium

We write the equation for hydrostatic equilibrium as Mihalas (1978, p. 170):

$$\frac{dP}{dm} = g. \tag{2.24}$$

P is the total pressure comprising gas, radiation and turbulent pressures, so that:

$$\frac{d}{dm}\left(NkT + \frac{4\pi}{c} \int_0^\infty f_\nu J_\nu\, d\nu + \frac{1}{2}\rho v_{\mathrm{turb}}^2 \right) = g \tag{2.25}$$

with Boltzmann's constant k and the turbulent velocity v_{turb}. The hydrostatic equation may either be solved simultaneously with all other equations or separately between iterations. The overall convergence behavior is usually the same in both cases. If taken into the linearization scheme, and a local $\Lambda^\star$ operator is used, then, as in the case of the radiative equilibrium equation, explicit depth-coupling enters via the depth derivative d/dm. Again,

solution of the linearized equations must proceed inwards starting at the outer boundary. The starting value at the first depth point (subscript $d = 1$) is:

$$N_1 k T_1 + \frac{1}{2}\rho_1 v_{\rm turb}^2(m_1) = m_1 \left(g - \frac{4\pi}{c} \int_0^\infty \frac{\chi_{1,\nu}}{\rho_1} h_\nu J_{\nu,k}\, d\nu \right), \tag{2.26}$$

where h_ν is the variable Eddington factor denoting the ratio of H_ν/J_ν at the surface, kept fixed during linearization.

We are also able to account for element separation resulting from pressure diffusion, which is the process that governs the spectroscopic appearance e.g. of white dwarfs. The numerical method and some results are described by Dreizler & Wolff (1999).

2.2.5 Particle-Conservation and Fictitious Massive-Particle Density

The total particle density N is the sum of electron density plus the populations of all atomic/ionic states, in all LTE and NLTE levels:

$$N = n_e + \sum_{k=1}^{NATOM} \sum_{l=1}^{NION(k)} \left[\sum_{i=1}^{NL(l)} n_{kli} + \sum_{i=1}^{LTE(l)} n^\star_{kli} \right]. \tag{2.27}$$

The fictitious massive-particle density n_H is introduced for notational convenience. It is defined by:

$$n_H = \sum_{k=1}^{NATOM} m_k \sum_{l=1}^{NION(k)} \left[\sum_{i=1}^{NL(l)} n_{kli} + \sum_{i=1}^{LTE(l)} n^\star_{kli} \right]. \tag{2.28}$$

The mass of a chemical species in AMU is denoted by m_k. Introducing the mass of a hydrogen atom m_H, we may write the material density simply as

$$\rho = n_H m_H. \tag{2.29}$$

2.2.6 Opacity and Emissivity

Thermal opacity and emissivity are made up by radiative bound-bound, bound-free and free-free transitions. For each species we compute and sum:

$$\begin{aligned}\kappa_\nu &= \sum_{l=1}^{NION}\left[\sum_{i=1}^{NL(l)}\sum_{j>i}^{NL(l)}\sigma_{li\to lj}(\nu)\left(n_{li}-n_{lj}\frac{g_{li}}{g_{lj}}e^{-h(\nu-\nu_{ij})/kT}\right)\right. \\ &+\sum_{i=1}^{NL(l)}\sum_{j>i}^{NL(l+1)}\sigma_{li\to l+1,k}(\nu)\left(n_{li}-n^\star_{li}e^{-h\nu/kT}\right) \\ &\left.+\,n_e\sigma_{kk}(l,\nu)\left(1-e^{-h\nu/kT}\right)\left(\sum_{i=1}^{NL(l+1)}n_{l+1,i}+\sum_{i=1}^{LTE(l+1)}n^\star_{l+1,i}\right)\right]\end{aligned} \tag{2.30}$$

where the total opacity includes Thomson scattering, i.e. $\chi_\nu = \kappa_\nu + n_e\sigma_e$, and

$$\begin{aligned}\frac{\eta_\nu}{2h\nu^3/c^2} &= \sum_{l=1}^{NION}\left[\sum_{i=1}^{NL(l)}\sum_{j>i}^{NL(l)}\sigma_{li\to lj}(\nu)n_{lj}\frac{g_{li}}{g_{lj}}e^{-h(\nu-\nu_{ij})/kT}\right. \\ &+\sum_{i=1}^{NL(l)}\sum_{j>i}^{NL(l+1)}\sigma_{li\to l+1,k}(\nu)n^\star_{li}e^{-h\nu/kT} \\ &\left.+\,n_e\sigma_{kk}(l,\nu)e^{-h\nu/kT}\left(\sum_{i=1}^{NL(l+1)}n_{l+1,i}+\sum_{i=1}^{LTE(l+1)}n^\star_{l+1,i}\right)\right].\end{aligned} \tag{2.31}$$

$\sigma_{li\to l+1,k}(\nu)$ denotes the cross-section for photoionization from level i of ion l into level k of ion $l+1$. The double summation over the bound-free continua takes into account the possibility that a particular level may be ionized into more than one level of the next high ion. Again, note the definition of the LTE population number $n^\star_{li}$ in this case, which depends on the level $(l+1,k)$ of the parent ion:

$$n^\star_{li} = n_{l+1,k}n_e\phi_{li}\frac{\phi_{l+1,1}}{\phi_{l+1,k}}. \tag{2.32}$$

Note also that the concept of LTE levels (whose occupation numbers enter, e.g. the number- and charge-conservation equations) in the atomic models of complex ions is therefore not unambiguous. Our code always assumes that LTE levels in the model atoms are populated in LTE with respect to the ground state of the upper ion.

The source function used for the approximate radiation transfer is η_ν/κ_ν, thus it excludes Thomson scattering. For the exact formal solution of course, the total opacity χ_ν in the expression Eq. 2.4 includes the Thomson term $(n_e\sigma_e)$.

2.2.7 Atomic Level Dissolution by Plasma Perturbations

As high-lying atomic levels are strongly perturbed by other charged particles in the plasma they are broadened and finally dissolved. This effect is observable by line merging at series limits and must be accounted for in line profile analyses. Moreover, line-overlap couples the radiation field in many lines and flux-blocking can strongly affect the global atmospheric structure. Numerically, we treat the level dissolution in terms of occupation probabilities, which for LTE plasmas can be defined as the ratio of the level populations to those in absence of perturbations. A phenomenological theory for these quantities was given in Hummer & Mihalas (1988). The non-trivial generalization to NLTE plasmas was made by Hubeny et al. (1994). In practice an individual occupation-probability factor (depending on T, n_e, and principal quantum number), is applied to each atomic level, which describes the probability that the level is dissolved. Furthermore, the rate equations Eq. 2.11 must be generalized in a unique and unambiguous manner. For details see Hubeny et al. (1994).

2.3 The Accelerated Lambda Iteration (ALI)

In practice, however, an optimum choice is desired in order to achieve convergence with a minimum amount of iteration steps. The history of the ALOs is interesting, and was summarized in detail by Hubeny (1992). Of utmost importance were two papers by Olson and collaborators (Olson et al. 1986, Olson & Kunasz 1987) who overcame the major drawback of early ALOs, namely the occurrence of free parameters controlling the convergence process, and thus found the optimum choice of ALOs. Our model atmosphere program permits the use of either a diagonal or a tri-diagonal ALO, both are set up following Olson & Kunasz (1987).

2.3.1 Diagonal (Local) Lambda Operators

In this case the mean intensity J_d at a particular depth d in the current iteration step is computed solely from the local source function S_d and a correction term ΔJ_d, the latter depending on the source functions (at all depths) from the previous iteration. Dropping the iteration count and introducing indices denoting depth points we can write:

$$J_d = \Lambda^\star_{d,d} S_d + \Delta J_d. \tag{2.33}$$

In discrete form we can think of $\Lambda^\star$ as a matrix acting on a vector whose elements comprise the source functions of all depths. Then $\Lambda^\star_{d,d}$ is the diagonal element of the $\Lambda^\star$ matrix corresponding to depth point d. Writing $\Lambda^\star_{d,d} \equiv B_d$ (for numerical computation see Eq. 2.37 below) we have a purely local expression for the mean intensity:

$$J_d = B_d S_d + \Delta J_d. \tag{2.34}$$

2.3.2 Tridiagonal (Non-local) Lambda Operators

Much better convergence is obtained if the mean intensity is computed not only from the local source function, but also from the source function of the neighboring depths points. Then the matrix representation of $\Lambda^\star$ is of tri-diagonal form and we may write:

$$J_d = C_{d-1} S_{d-1} + B_d S_d + A_{d+1} S_{d+1} + \Delta J_d \ , \tag{2.35}$$

where C_{d-1} and A_{d+1} represent the upper and lower subdiagonal elements of $\Lambda^\star$, and $S_{d\pm1}$ the source functions at the adjacent depths. By analogy the correction term becomes:

$$\Delta J_d = \Lambda_{d,d'} S_{d'} - (C_{d-1} S_{d-1} + B_d S_d + A_{d+1} S_{d+1}). \tag{2.36}$$

Again all quantities for the computation of ΔJ_d are known from the previous iteration, and the first term gives the exact formal solution of the transfer equation. We emphasize again that the source functions in Eq. 2.35 are to be computed from the correct occupation numbers and temperature, all of which are still unknown. We therefore have a non-linear set of equations for these quantities, which must be solved by either Newton-Raphson iteration or other techniques, resulting in the solution of a tri-diagonal linear equation.

As was shown in Olson et al. (1986) the elements of the optimum $\Lambda^\star$ matrix are given by the corresponding elements of the exact Λ matrix. The diagonal and subdiagonal elements are computed following Olson & Kunasz (1987):

$$\begin{aligned} A_{d+1} &= \int_0^1 \left(e^{-\Delta\tau_d} \frac{e^{-\Delta\tau_{d-1}} - 1}{\Delta\tau_{d-1}} - \frac{e^{-\Delta\tau_d} - 1}{\Delta\tau_d} \right) \frac{d\mu}{2}, \\ 1 - B_d &= \int_0^1 \left(\frac{1 - e^{-\Delta\tau_{d-1}}}{\Delta\tau_{d-1}} + \frac{1 - e^{-\Delta\tau_d}}{\Delta\tau_d} \right) \frac{d\mu}{2}, \\ C_{d-1} &= \int_0^1 \left(e^{-\Delta\tau_{d-1}} \frac{e^{-\Delta\tau_d} - 1}{\Delta\tau_d} - \frac{e^{-\Delta\tau_{d-1}} - 1}{\Delta\tau_{d-1}} \right) \frac{d\mu}{2}, \end{aligned} \tag{2.37}$$

with $\Delta\tau_{d-1} \equiv (\tau_d - \tau_{d-1})/\mu$. At large optical depths with increasing $\Delta\tau$ steps (the depth grid is roughly equidistant in $\log\tau$) the subdiagonals A_{d+1} and C_{d-1} vanish, and the diagonal B_d approaches unity, reflecting the fact that the radiation field is more and more determined by local properties of the matter. At very small optical depths all elements of $\Lambda^\star$ vanish, reflecting the non-localness of the radiation field at these depths.

2.3.3 Acceleration of Convergence

To accelerate the convergence of the iteration, the scheme originally proposed by Ng (1974) and later by Auer (1987) has been implemented. It extrapolates the correction vector $\delta\boldsymbol{\psi}_d$ from the previous three iterations. From our experience the extrapolation often yields over-corrections, resulting in alternating convergence or even divergence. In contrast, use of a tri-diagonal ALO usually results in satisfactorily fast convergence, so that the acceleration scheme is rarely used.

2.4 Solution of the Non-linear Equations by Iteration

2.4.1 Discretization

After a depth-grid is chosen, we start by computing a gray LTE continuum model using the Unsöld-Lucy temperature-correction procedure. Depth points (typical number is 90) are chosen in equidistant steps on a logarithmic (Rosseland) optical depth scale. The converged LTE model (temperature and density structure, given on a column mass depth

scale) is written to a file that is read by PRO2. The NLTE code uses the column mass as an independent depth variable.

The frequency grid is determined by the atomic-data input file. Frequency points are set blue- and red-ward of each absorption edge, and for each spectral line. Gaps are filled up by setting continuum points. Finally, the quadrature weights are computed. Frequency integrals appearing e.g. in Eq. 2.23 are replaced by quadrature sums, and depth derivatives by difference quotients.

2.4.2 Linearization

All variables x are replaced by $x \rightarrow x + \delta x$ where δx denotes a small perturbation of x. Terms not linear in these perturbations are neglected. The perturbations are expressed by perturbations of the basic variables:

$$\delta x = \frac{\partial x}{\partial T}\delta T + \frac{\partial x}{\partial n_e}\delta n_e + \frac{\partial x}{\partial N}\delta N + \frac{\partial x}{\partial n_H}\delta n_H + \sum_{l=1}^{NL}\frac{\partial x}{\partial n_l}\delta n_l. \tag{2.38}$$

As an illustrative example we linearize the equation for radiative equilibrium. Most other linearized equations may be found in Werner (1986). Assigning two indices (d for depth and i for frequency of a grid with NF points) to the variables and denoting the quadrature weights with w_i Eq. 2.23 becomes:

$$\sum_{i=1}^{NF} w_i\left(\frac{\chi_{di}}{\bar{\kappa}_J}[\delta S_{di} - \delta J_{di}] + \delta\chi_{di}[S_{di} - J_{di}]\right) + \bar{\Lambda}^\star_J \sum_{i=1}^{NF}\frac{w_i}{\Delta\tau_i}(\delta J_{di} f_{di} - \delta J_{d-1,i} f_{d-1,i})$$

$$= F_0 + \bar{\Lambda}^\star_J \mathcal{H} - \sum_{i=1}^{NF} w_i \frac{\chi_{di}}{\bar{\kappa}_J}(S_{di} - J_{di}) - \bar{\Lambda}^\star_J \sum_{i=1}^{NF}\frac{w_i}{\Delta\tau_i}(f_{di} J_{di} - f_{d-1,i} J_{d-1,i}). \tag{2.39}$$

Note that we do not linearize $\Delta\tau_i$. Because of this, convergence properties may deteriorate significantly in some cases. Perturbations $\delta S_{di}, \delta\chi_{di}$ are expressed by Eq. 2.38, and the perturbation of the mean intensity J_{di} is, according to Eq. 2.35, given through the perturbations of the source function at the current and the two adjacent depths:

$$\delta J_{di} = C_{d-1,i}\delta S_{d-1,i} + B_{di}\delta S_{di} + A_{d+1,i}\delta S_{d+1,i}\ , \tag{2.40}$$

where A, B, C are the Λ matrix elements from Eq. 2.37. The $\delta J_{d-1,i}$ contain the term $C_{d-2,i}\delta S_{d-2,i}$ which is neglected because we want to account only for nearest neighbor coupling. We write δS_{di} with the help of Eq. 2.38 and observe that for any variable z:

$$\frac{\partial S_{di}}{\partial z} = \frac{1}{\chi_{di}} \left(\frac{\partial \eta_{di}}{\partial z} - S_{di} \frac{\partial \chi_{di}}{\partial z} \right). \tag{2.41}$$

Derivatives of opacity and emissivity with respect to temperature, electron and population densities are computed from analytical expressions (see e.g. Mihalas et al. 1975, Werner 1987). We finally get from Eq. 2.39:

$$\begin{aligned}
&\delta T_{d-1,i} \left\{ \sum_i^{NF} -\frac{w_i}{\bar{\kappa}_J} \frac{\partial S_{d-1,i}}{\partial T} \chi_{di} C_{d-1,i} \right. \\
&\left. + \bar{\Lambda}^\star_J \sum_i^{NF} \frac{w_i}{\Delta\tau_i} (f_{di} C_{d-1,i} - f_{d-1,i} B_{d-1,i}) \frac{\partial S_{d-1,i}}{\partial T} \right\} + \\
&\delta T_d \left\{ \sum_i^{NF} \frac{w_i}{\bar{\kappa}_J} \left[\frac{\partial S_{di}}{\partial T} \chi_{di} (1 - B_{di}) + \frac{\partial \chi_{di}}{\partial T} (S_{di} - J_{di}) \right] \right. \\
&\left. + \bar{\Lambda}^\star_J \sum_i^{NF} \frac{w_i}{\Delta\tau_i} (f_{di} B_{di} - f_{d-1,i} A_{di}) \frac{\partial S_{di}}{\partial T} \right\} + \\
&\delta T_{d+1,i} \left\{ \sum_i^{NF} -\frac{w_i}{\bar{\kappa}_J} \frac{\partial S_{d+1,i}}{\partial T} \chi_{di} A_{d+1,i} \right. \\
&\left. + \bar{\Lambda}^\star_J \sum_i^{NF} \frac{w_i}{\Delta\tau_i} (f_{di} A_{d+1,i} - f_{d-1,i} B_{d+1,i}) \frac{\partial S_{d+1,i}}{\partial T} \right\} + \\
&\delta n_{e_{d-1,i}} \{\cdots\} + \delta n_{e_{d,i}} \{\cdots\} + \delta n_{e_{d+1,i}} \{\cdots\} + \\
&\sum_{l=1}^{NL} \delta n_{l_{d-1,i}} \{\cdots\} + \sum_{l=1}^{NL} \delta n_{l_{d,i}} \{\cdots\} + \sum_{l=1}^{NL} \delta n_{l_{d+1,i}} \{\cdots\} \\
&= \text{r.h.s.}
\end{aligned} \tag{2.42}$$

The curly brackets $\{\cdots\}$ denote terms that are similar to those multiplied by perturbations of the temperature. Instead of partial derivatives with respect to T, they contain derivatives with respect to n_e and the populations n_l. They all represent coefficients of the matrices $\boldsymbol{\alpha}, \boldsymbol{\beta}, \boldsymbol{\gamma}$ in Eq. **??**.

2.4.3 Newton-Raphson Iteration

As described above, the linearized equations have a tri-diagonal block-matrix form, see Eq. **??**. Inversion of the grand matrix ($\equiv \mathbf{T}$ sized $(NN \cdot ND) \times (NN \cdot ND)$, i.e. about $10^4 \times 10^4$ in typical applications) is performed with a block-Gaussian elimination scheme, which means that our iteration of the non-linear equations is a multi-dimensional Newton-Raphson method. The problem is structurally simplified when explicit-depth coupling is avoided by the use of a local ALO, however, the numerical effort is not reduced much, because in both cases the main effort lies with the inversion of matrices sized $NN \times NN$. The Newton-Raphson iteration involves two numerically expensive steps, first setting up the Jacobian (comprising $\boldsymbol{\alpha}, \boldsymbol{\beta}, \boldsymbol{\gamma}$) and then inverting it. Additionally, the matrix inversions in Eq. **??** limit their size to about $NN = 250$ because otherwise numerical accuracy is lost. Two variants recently introduced in stellar atmosphere calculations are able to improve both numerical accuracy and, best of all, computational speed.

2.4.4 Alternative Fast Solution Techniques for Non-linear Equations: Broyden– and Kantorovich–variants

Broyden's (1965) variant belongs to the family of quasi-Newton methods; it was first used in model-atmosphere calculations in Dreizler & Werner (1991), Hamann et al. 1991, Koesterke et al. (1992). It avoids the repeated set-up of the Jacobian by the use of an update formula. In addition, it also gives an update formula for the *inverse* Jacobian. In the case of a local ALO the solution of the linearized system at any depth is:

$$\delta\boldsymbol{\psi_k} = \boldsymbol{\beta}_k^{-1}\,\mathbf{c_k}. \tag{2.43}$$

Let $\boldsymbol{\beta}_k^{-1}$ be the k-th iterate of the inverse Jacobian, then an update can be found from:

$$\boldsymbol{\beta}_{k+1}^{-1} = \boldsymbol{\beta}_k^{-1} + \frac{(\mathbf{s}_k - \boldsymbol{\beta}_k^{-1}\mathbf{y}_k)\otimes(\mathbf{s}_k^T\boldsymbol{\beta}_k^{-1})}{\mathbf{s}_k^T\boldsymbol{\beta}_k^{-1}\mathbf{y}_k}, \tag{2.44}$$

where $\otimes$ denotes the dyadic product, and where we have defined:

$$\mathbf{s}_k \equiv \quad \delta\boldsymbol{\psi}_k \qquad \text{solution vector of preceding linearization,}$$

$$\mathbf{y}_k \equiv \quad \mathbf{c}_{k+1} - \mathbf{c}_k \qquad \text{difference of actual and preceding residuum.}$$

The convergence rate is super-linear, i.e. slower than the quadratic rate of the Newton-Raphson method; but this is more than compensated by the tremendous speed-up for a single iteration step. It is not always necessary to begin the iteration with the calculation of an exact Jacobian and its inversion. Experience shows that in an advanced stage of the overall (ALI-) iteration (i.e. when corrections become small, of the order 1%) we can start the linearization cycle Eq. 2.44 by using the inverse Jacobian from the previous overall iteration. Computational speed-up is extreme in this case, however, it requires storage of the Jacobians of all depths.

More difficult is its application to the tri-diagonal ALO case. Here we have to update the grand matrix $\mathbf{T}$ which, as already mentioned, is of block tri-diagonal form. We cannot update its inverse, because it is never computed explicitly. Furthermore we need an update formula that preserves the block tri-diagonal form which is a prerequisite for its inversion by the Feautrier scheme. Such a formula was found by Schubert (1970):

$$\mathbf{T}_{k+1} = \mathbf{T}_k + \frac{(\mathbf{y}_k - \mathbf{T}_k \mathbf{s}_k) \otimes \bar{\mathbf{s}}_k^T}{\bar{\mathbf{s}}_k^T \bar{\mathbf{s}}_k}, \tag{2.45}$$

where $\bar{\mathbf{s}}_k \equiv \mathbf{Z}\mathbf{s}_k$ with the structure matrix $\mathbf{Z}$ as defined by:

$$Z_{ij} = \begin{cases} 1 & \text{if} \quad T_{ij} \neq 0 \\ 0 & \text{if} \quad T_{ij} = 0. \end{cases}$$

The vectors $\mathbf{s}_k$ and $\mathbf{y}_k$ are defined as above but now they span quantities over all depth instead of a single depth point. With this formula we obtain new submatrices $\boldsymbol{\alpha}, \boldsymbol{\beta}, \boldsymbol{\gamma}$ and $\mathbf{c}$ with which the Feautrier scheme is solved again. This procedure saves the computation of derivatives. Another feature realized in our program also saves the repeated inversion of $\mathbf{q} \equiv (\boldsymbol{\beta}_d + \boldsymbol{\gamma}_d \mathbf{D}_{d-1})$ by updating its inverse with the Broyden formula Eq. 2.44. Similar to the diagonal ALO case it is also possible to pass starting matrices from one overall iteration to the next for the update of $\mathbf{T}$ and the matrix $\mathbf{q}^{-1}$. In both cases the user specifies two threshold values for the maximum relative correction in $\delta\boldsymbol{\psi}$ which cause the program to switch from Newton-Raphson to Broyden stages 1 and 2. During stage 1, each new overall cycle is started with an exact calculation and inversion of all matrices involved, and in stage 2 these matrices are passed through each iteration.

Chapter 3

NLTE Model Stellar Atmospheres for Different Spectral Types

3.1 Introduction

As was stated before, the observed spectrum is practically the only information about a star we have. The process of deducing stellar properties from its spectrum is therefore called spectroscopic diagnostics. This is a multi-step process with many interlinked steps. An example for spectral diagnostic of DO white dwarfs is schematically displayed in Figure (3.1).

The basic step is input physics. By this term we mean a selection of the basic physical assumptions under which the medium is being described (i.e., which processes and phenomena are neglected; which equilibrium conditions are assumed to hold, etc.). The basic assumptions then determine the equations to be solved. They also tell us what are the basic input parameters of the model construction. For instance, when adopting the assumption of a plane-parallel atmosphere in the hydrostatic and radiative equilibrium, the input model parameters are the effective temperature, surface gravity, and chemical composition. These parameters are basic from the point of constructing model atmospheres, yet they are related to other parameters which may be viewed as more fundamental, like stellar mass, radius, and luminosity. The latter parameters are fundamental if one considers a certain instant of the stellar life. Taking into account more extended input physics (i.e., adding the stellar evolution theory), we may then consider even more fundamental

parameters like the initial stellar mass, initial composition, and the age. Likewise, go-

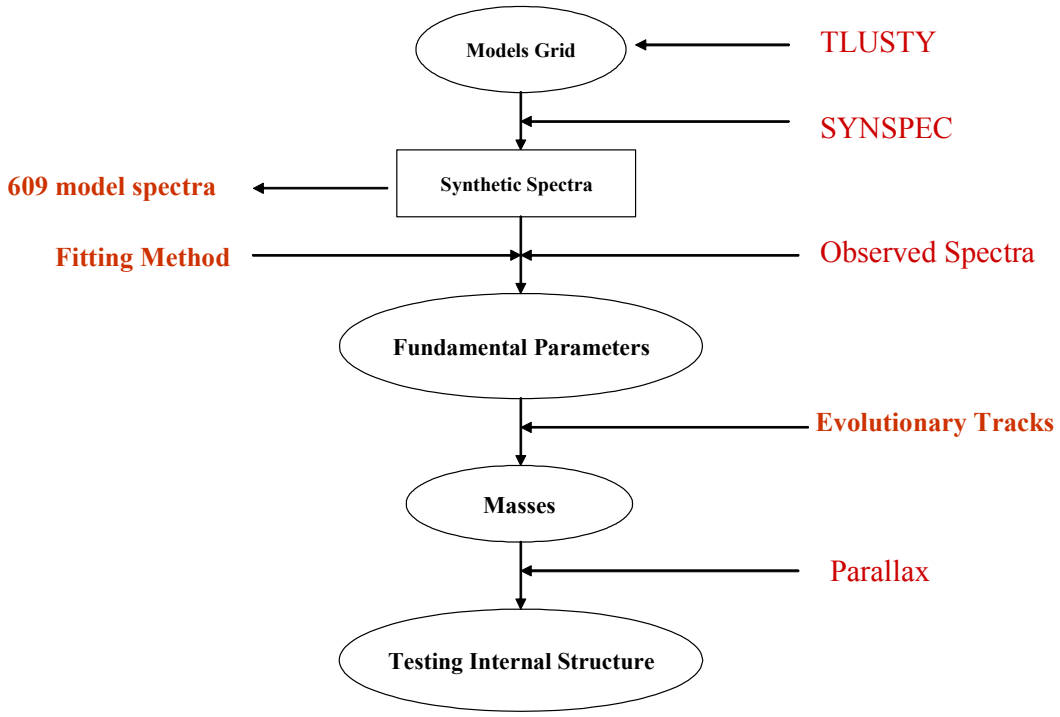

Figure 3.1: **A sketch of the individual steps of astrophysical spectroscopic diagnostics of DO white dwarfs, Nouh and Fouda (2007).**

ing to more complex models, like for instance the unified photosphere wind models, we have different input parameters depending on the level of physical description we adopt. In a simple theory we have, in addition to the stellar mass, radius, and luminosity, two additional input parameters, the mass loss rate and the wind terminal velocity. In a more involved physical picture we may come up with a relation between the wind parameters and other parameters. Sometimes the additional input parameters make up for the lack

of adequate physics. Typical examples are the so-called microturbulent velocity which is often used for describing short-scale non-thermal motions; or the mixing length parameter used in the mixing-length theory of convection.

In the following sections, main results of the calculations of NLTE model for different regions on the HR diagram are summarized.

3.2 The Solar Atmosphere

The Sun offers an ideal test-bench for model atmospheres. Our ability to resolve its surface means highly-detailed data can be obtained. While the solar 1D LTE models have been tested against many diagnostics, this is not the case for the new generation of models (3D LTE and 1D NLTE).

Anderson (1989) computed a line-blanketed NLTE model in hydrostatic and radiative equilibrium for the Sun, noting significant differences in the atmospheric structure with respect to LTE for $\tau \lesssim 10^{-3}$. Hauschildt, Allard, & Baron (1999) computed consistent NLTE model atmospheres for the Sun, finding small differences between LTE and NLTE structures. However, their calculations treated neither Al I nor Mg I in NLTE.

Pereira (2009) tests the temperature structure and find a surprisingly good agreement between the 3D model and the observations, surpassing even semi-empirical models. The solar 1D non-LTE models have a very similar behaviour to 1D LTE models, confirming that LTE is a good approximation in the solar photosphere. The 3D theoretical model performs consistently better than its 1D counterparts.

In Figure (3.2) the mean temperature structure of the 3D model is plotted against the phoenix LTE and NLTE models. The effect of NLTE in the phoenix models seems to be a cooling of the outer layers, with minor differences at other depths. This NLTE cooling goes in the opposite direction of the NLTE effects of other phoenix solar NLTE models (Short & Hauschildt, 2005, 2009), where the NLTE effects cause a warming in the outer layers. This discrepancy seems to be associated with a different choice of atomic species treated in NLTE.

So, one can summarize that, the solar NLTE models indicate that the NLTE effects on

the atmospheric structure are small (< 200 K in the outer layers), which confirms LTE as a good approximation for the solar photosphere.

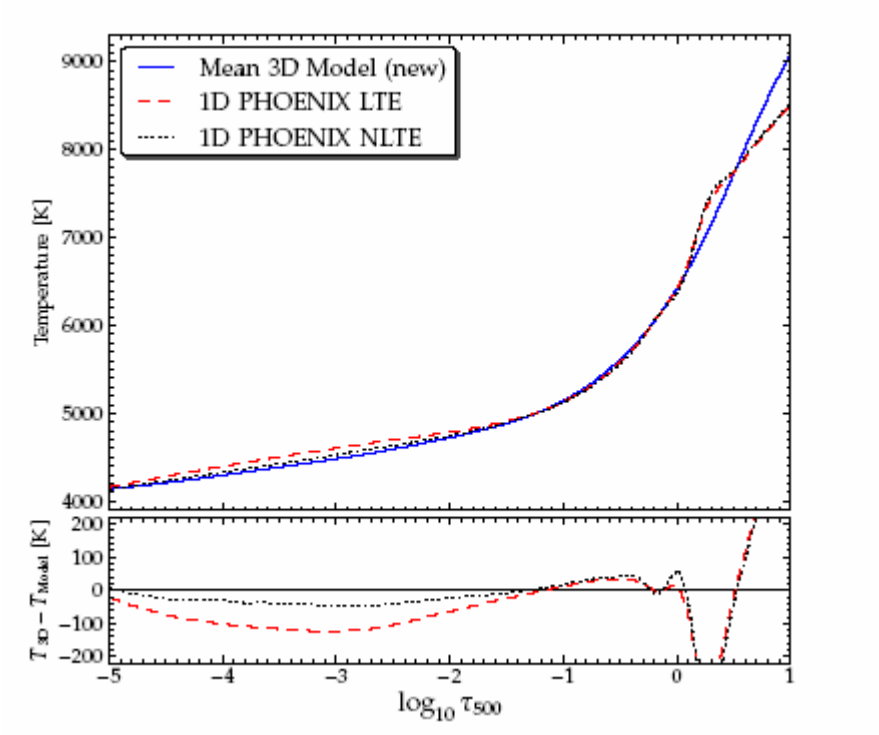

Figure 3.2: **Temperature structure for different models plotted against the optical depth at 500 nm.**

3.3 Early Type Stars

Atmospheres of early-type stars have played, and continue to play, an important role not only in the stellar atmosphere theory, but in overall astrophysical radiative transfer theory in general. The whole non-LTE theory was first developed and tested on early-type stellar atmospheres. Consequently, modelling early-type stellar atmospheres is a mature field, which may serve as a methodological guide to other astrophysical objects where the

radiation also plays an important role, as, for instance, accretion disks in Active Galactic Nuclei (AGN) and in Cataclysmic Variables (CV), HII regions, and others.

During the last three decades, it was demonstrated that departures from LTE are crucial for spectroscopic studies of early-type stars, even the photospheric layers. Early non-LTE models were constructed already in the late 1960's and in the first half of the 1970's by Mihalas and coworkers. Nevertheless, the numerical problems and sheer amount of computer time and memory needed for computing non-LTE metal line-blanketed model atmospheres have precluded computing such models until the late 1980's. Because sufficiently efficient computer codes for mass production of non-LTE line-blanketed models were being developed only during mid 1990's, there is no comprehensive grid of non-LTE line blanketed models, which would cover the same range of parameters as the Kurucz grid, currently available, but they will very likely be built in the forthcoming years.

From the practical point of view, the most important result of model atmospheres is the prediction of emergent radiation, which is then compared to the observed spectrum in order to deduce basic stellar parameters.

One of the most promising NLTE codes is TLUSTY (Hubeny, 1988). Based on this code, grids for O-type (OSTAR2002, Lanz & Hubeny, 2003) and B-types (BSTARS2006, Lanz & Hubeny, 2007) atmospheres are already published. The discussion in the next two subsections will lie on these grids.

3.3.1 O-type Stars

Figures (3.3) displays the NLTE ionization fractions of all explicit species, along with LTE fractions (for a direct comparison), the LTE fractions are computed by the Saha formula for temperature and density distributions of the NLTE models. The behavior of individual species is different, but we can see a general trend: the fractions of dominant ions are usually not sensitive to NLTE effects (that is, they are close to unity in both LTE and NLTE). The fractions of ions with lower ionization degrees are typically lower in NLTE because these ions are overionized by the strong radiation field that originates in deep, very hot layers (notice that the recombination rate is given through the local temperature). Conversely,

higher ionization degrees are typically larger in NLTE. This ionization shift is one of the most important NLTE effects in hot star atmospheres.

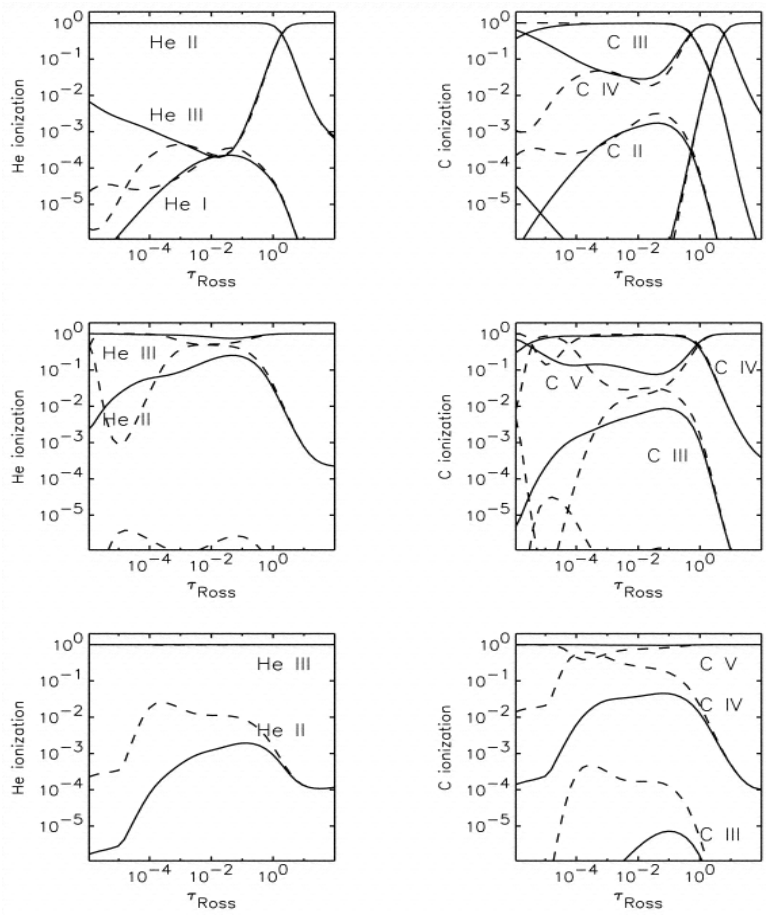

Figure 3.3: **Ionization fractions of helium and carbon in three model atmospheres, Teff = 30,000 (top), 40,000 (middle), and 50,000 K (bottom), log g = 4.0, and solar composition. LTE ionization is shown with dashed lines.**

In Figure (3.4), NLTE model fluxes are compared to Kurucz (1993) models. Because of different averaging procedures used in both sets of model spectra, the comparison is not exact but nevertheless shows the general effect. Three models are computed for (Teff, log g) pairs equal to (40,000, 4.5), (35,000, 4.0), and (30,000, 4.0), as well as for solar metallicity. The agreement between these models and Kurucz models is very good in the optical spectrum for all three models (bottom panel). For Teff = 30,000 K the agreement

between OSTAR2002 and Kurucz fluxes is rather good in the UV spectrum, while for the hotter models, NLTE flux is lower.

In contrast, NLTE models predict higher flux than Kurucz models in the Lyman continuum, although the effect is relatively small at 40,000 K.

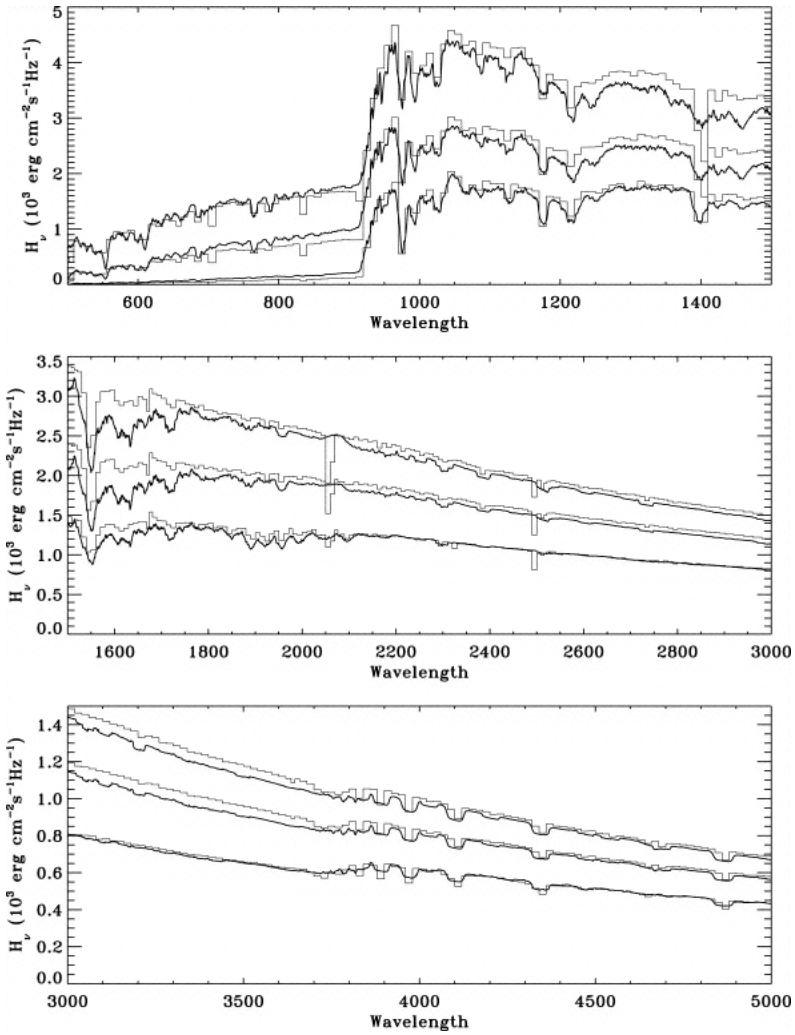

Figure 3.4: **Predicted flux for three model atmospheres with (Teff, log g) equal to (40,000 K, 4.5), (35,000 K, 4.0), and (30,000 K, 4.0) (thick lines), compared to Kurucz models with the same parameters (thin histograms). Different panels show different spectrum regions.**

3.3.2 B-type Stars

As O-type stars, the comparison is done between the atmospheric structure of NLTE BSTAR2006 and LTE Kurucz (1993) model atmospheres. Figure (3.5) displays the temperature stratification of a series of solar composition and one-tenth solar metallicity NLTE and LTE models, Teff = 25,000 K, log g = 3.0 and 4.0. At large depths where the departures from LTE are small, the LTE and NLTE atmospheric temperature structures are very similar. In shallower layers, the local temperature in NLTE models is higher than in the LTE models. In the NLTE models, temperature is basically determined by a balance between heating by the Balmer hydrogen lines and cooling by lines of heavy elements (carbon and heavier elements). Also, Figure (3.5) illustrates that the classical NLTE temperature rise is not completely removed by the cooling from metal lines, even at solar metallicity, and shows the metallicity dependence of this effect.

We may therefore expect from this comparison that LTE and NLTE continuum spectra will not differ too much, while the core of strong lines and lines from minor ions will be most affected by departures from LTE. Figure (3.6) displays a comparison of the predicted LTE and NLTE spectral energy distributions for three solar composition models with log g = 3.0 and Vt = 2 km s^{-1}. For this comparison, the spectra directly calculated by TLUSTY are used, but not detailed spectra computed by SYNSPEC. This figure reveals some differences in the continuum fluxes, most noticeably in the near ultraviolet, where the LTE fluxes are higher than the NLTE predictions. The lower NLTE fluxes result from the overpopulation of the H I (n = 2) level at the depth of formation of the continuum flux, hence implying a larger Balmer continuum opacity. A smaller difference is seen in the Paschen continuum of the cooler models because of overpopulation of the n = 3 level. At higher surface gravities, these differences are still present albeit reduced. To conserve the total flux, the LTE models show a lower flux in the far and extreme ultraviolet. In the hottest model shown (Teff = 25,000 K), the LTE prediction in the Lyman continuum in a factor of 2 lower than the NLTE flux. In the cooler models, the LTE flux is lower at wavelengths shorter than Lyman continuum.

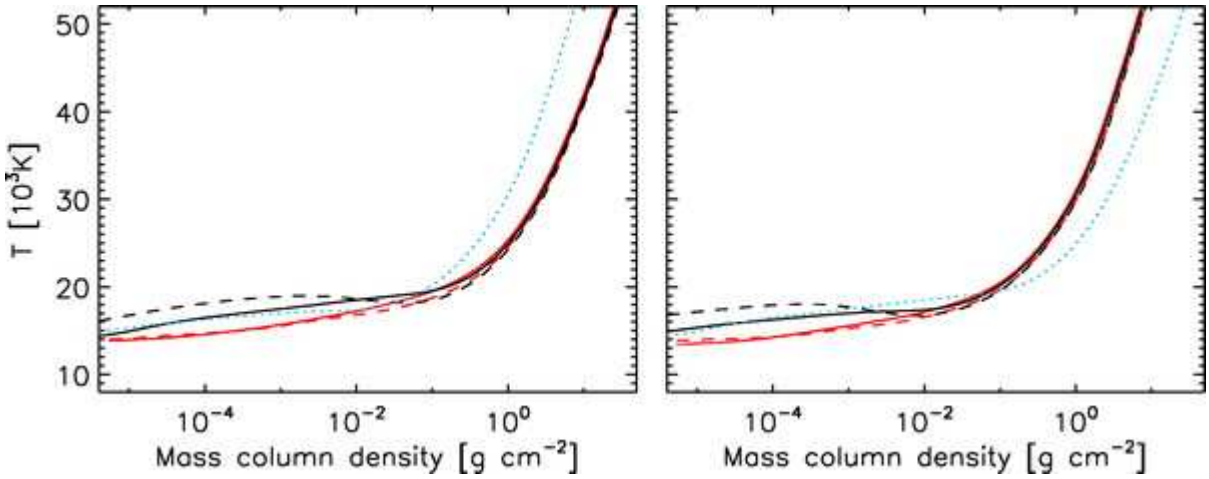

Figure 3.5: **Temperature structure of model atmospheres with Teff = 25,000 K, log g = 3.0 (left panel) and log g = 4.0 (right panel). Black lines show the temperature stratification of the NLTE BSTAR2006 models, compared to the LTE Kurucz models (grey lines). Solar composition models (full lines) and metal-poor (1/10 solar) models (dashed lines) are displayed. The dotted lines illustrate the effect of the different surface gravities.**

3.3.3 A-type Stars

Full NLTE model atmospheres of A-type stars are difficult to calculate, since the lines of different ions form at very different depths, and therefore there is a need for a huge amount of depth points to resolve all line formation regions sufficiently. Only LTE model atmospheres together with NLTE calculations for individual ions have been calculated in significant amounts. This underlines the need for more intensive calculations of NLTE model atmospheres of A-type stars. Adding consistently new different physical processes to standard model atmospheres for A-type stars and non-LTE effects to NLTE model atmospheres calculations, such as diffusion, magnetic fields, and more accurate treatment of convection zones, is necessary. This is the real challenging task the near future, Kubat & Korckov(2004).

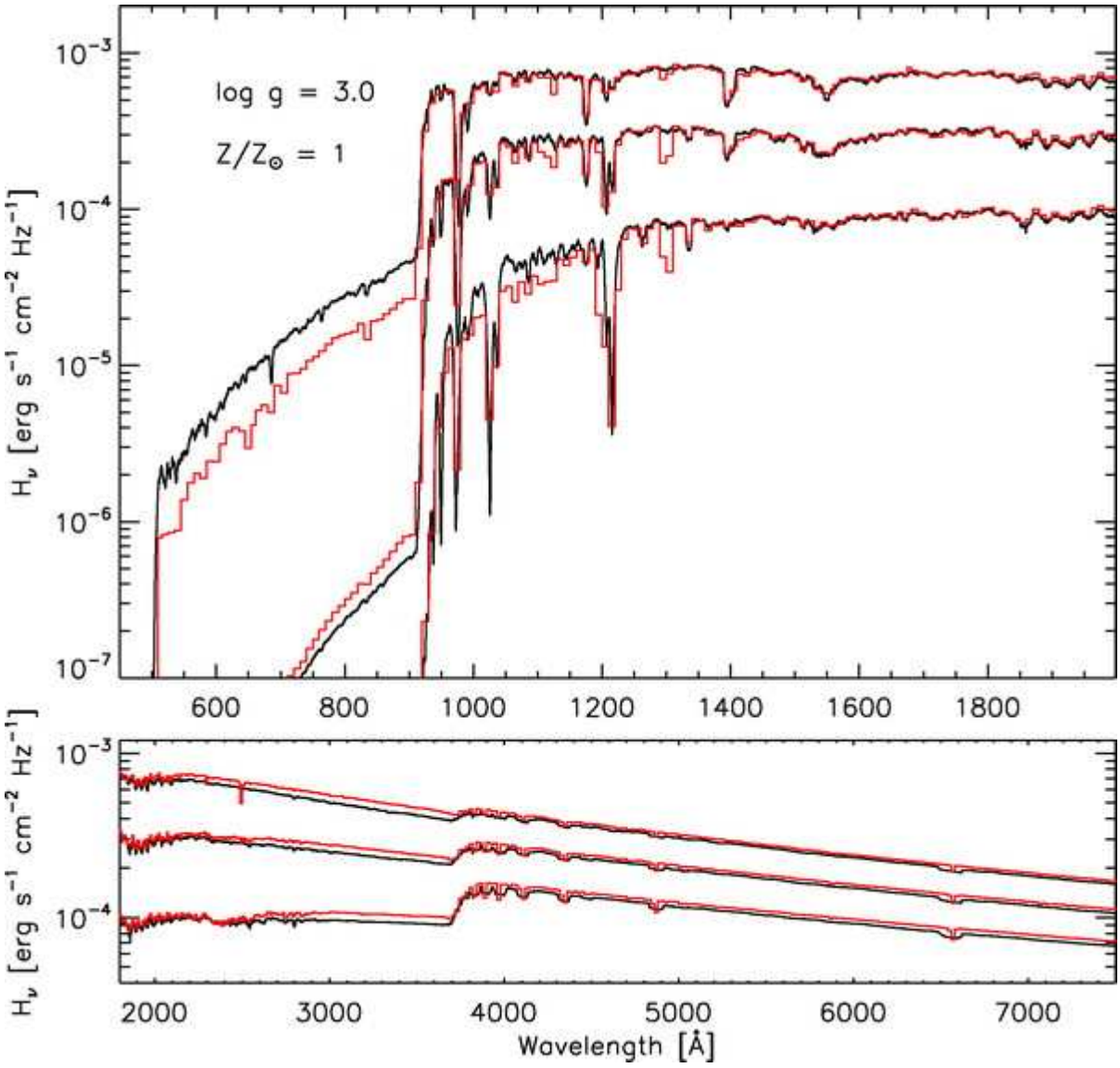

Figure 3.6: **Predicted flux for three solar composition model atmospheres with (Teff, log g) equal to (25,000 K, 3.0); (20,000 K, 3.0); and (15,000 K, 3.0) (black lines); compared to Kurucz (1993) models with the same parameters (grey lines).**

3.4 Late Type Stars

There exist mainly LTE models for late type stars but also some NLTE-calculations in order to determine the departure coefficients of several element lines have been done. NLTE effects change the profile of individual lines and in some cases they may change the structure of the spectrum itself significantly. For example, TiO forms a pseudo-continuum due to vibrational bands. Departures from LTE of the Ti I atom indirect changes the concentration of TiO.

Allende Priteto et al.(2003) presented NLTE calculations for the late type stars and found that, LTE and NLTE calculated fluxes systematically depart from observations below $\sim$ 1700 Å, where Si I bound-free absorption becomes very important.

From the comparison between observed and calculated fluxes between 2600 and 4000 Å, it is concluded that there is no solid foundation for previous claims of missing continuum opacity in the near-UV. It has also become apparent that departures from LTE will affect the shortest wavelengths, below $\sim$ 2600 Å. Coupling between the populations of different species that produce significant absorption in the UV is very likely, and detailed and simultaneous calculations for all of them are necessary.

The NLTE predictions for the species that play an important role in the UV, such as Al I or Mg I, fail to match the observed optical and near-infrared line profiles. In contrast, the NLTE profiles for Na I or O I, which do not absorb significantly in the UV, represent a clear improvement over their LTE counterparts, Figure (3.7). As the NLTE computations involve adopting a fixed LTE atmospheric structure (electron pressure and temperature and gas pressure), it seems a likely possibility that the adopted structure does not represent well the physical conditions in the highest atmospheric layers and, in turn, the level populations predicted in NLTE for UV-relevant species are wrong.

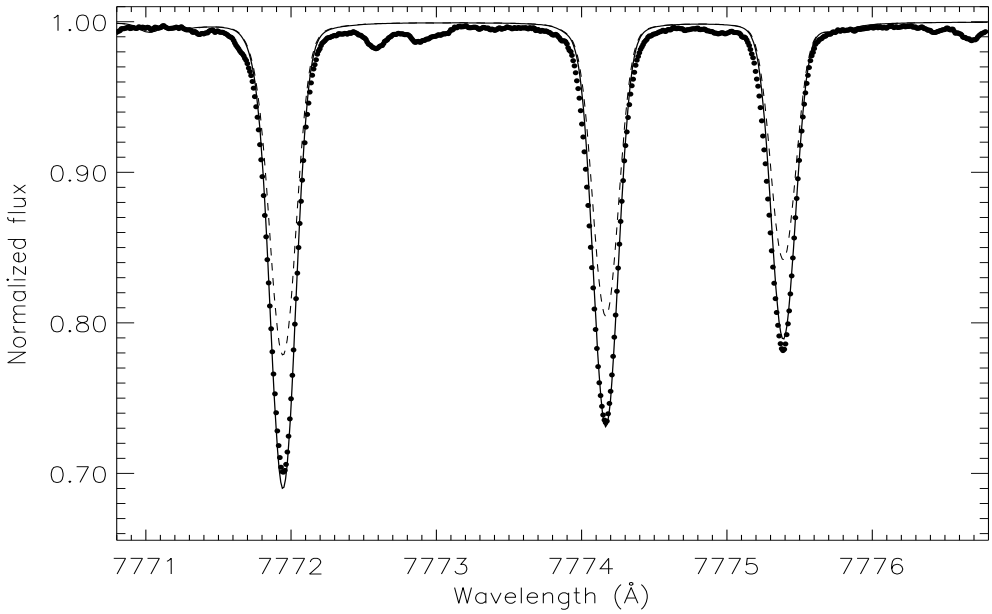

Figure 3.7: **Comparison between the observed (dots) and calculated line profiles for the O I infrared triplet. The solid line shows the NLTE calculation, and the dashed line shows the LTE profiles.**

3.5 White Dwarfs

White dwarfs can be divided into two basic distinct spectroscopic sequences, the DA and non-DA white dwarfs. DA white dwarfs display a pure hydrogen spectrum and can be found for all temperatures of the white dwarf cooling sequence, Koester (2002).

Non-DA white dwarfs comprises DO ($T_{eff} > 45000$ K), DB (11000 $K < T_{eff} <$ 30000 K) and DC ($T_{eff} < 11000$ K) white dwarfs. DO white dwarfs display a pure HeII lines spectrum at the hot end ($T_{eff} \geq 100000$ K) and HeI/HeII lines for the cool end. DB white dwarfs display a pure HeI lines spectrum. DC white dwarfs could be found for T_{eff} <11000 K and show featureless spectra (continuum spectra).

3.5.1 Helium White Dwarfs

The effect of NLTE on the calculation of model atmosphere were analyzed by Dreizler and Werner (1996) and Napiwotzki (1997). They found that, helium-rich DO white dwarfs have large differences for many important lines even at relatively low temperatures. This

prevents accurate LTE analysis for virtually all DO white dwarfs. So, the use of NLTE calculations is strongly recommended.

Kubat (1997) studied the effect of increasing helium abundance on the temperature structure of NLTE model atmospheres of hot white dwarfs with the effective temperature T_{eff} = 100000 K and log g = 7.5. He found quite dramatic changes in the temperature structure even for very low abundances of helium.

Hügelmyer et al. (2005) presented a grid of NLTE model atmosphere for a spectral analysis of DO white dwarfs from the Sloan Digital Sky Survey (SDSS).

Nouh and Fouda (2007) presented a grid of NLTE model atmospheres and synthetic spectra for hot rich-helium white dwarfs in order to elucidate the nature and characteristics of the progenitors of the DO white dwarfs. The grid coverage is $50000 \leq T_{eff} \leq 120000$ K with a step of 2500 K and $7 \leq \log g \leq 8.5$ with a step of 0.25 dex, for three helium abundance (by number relative to hydrogen) values (He/H): 10^2, 10^3 and 10^4. The spectra are synthesized with a sampling of 0.1 Å and covering the wavelength range from 3000 to 7000 Å.

The effect of the NLTE on the temperature stratification is displayed in Figure (3.8) for cool model at T_{eff} = 50000 K, $\log g = 8$ and He/H= 10^2, and in Figure (3.9) for hot model at T_{eff} = 100000 K, $\log g = 8$ and He/H= 10^2, the effect is significant for the layers near the surface where the optical spectra originate, while at large depths ($\tau_{Ross} \geq 1$), the departure from LTE is small and so the LTE and NLTE atmospheric structures are similar, Nouh and Fouda(2007).

Also, Naptwoski(1997) observed that, there are significant difference between the line profile calculated at LTE and that calculated at NLTE, Figure (3.10)

3.5.2 Hydrogen White Dwarfs

NLTE and LTE models for DA white dwarfs are in perfect agreement for temperatures up to 70000 K. This means that nearly all DA white dwarfs, except a few extraordinary hot ones, are accessible to LTE techniques. The situations becomes completely different, however, as soon as traces of helium are present in the atmosphere. As Bergeron et al. (1994) have

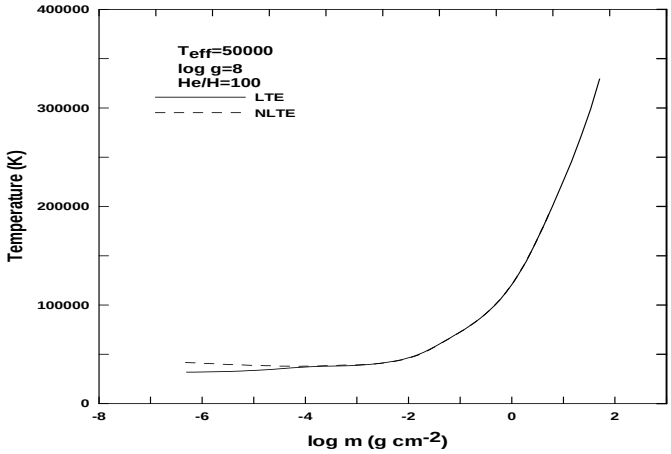

Figure 3.8: **The temperature stratification for the NLTE model for DO white dwarfs at** 50000 **K,** $\log g = 8$**, He/H=** 10^2**.**

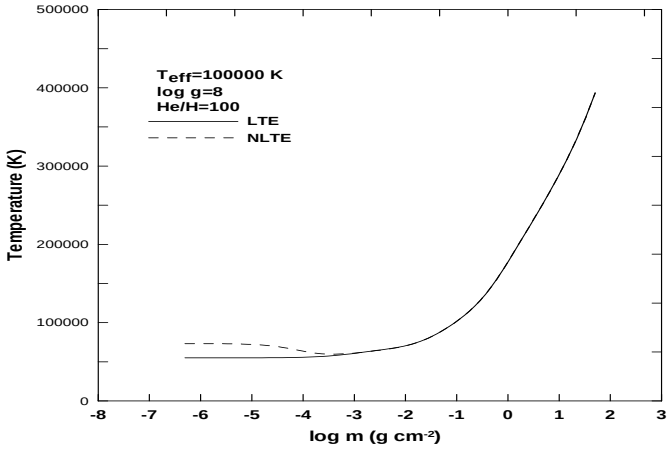

Figure 3.9: **The temperature stratification for the NLTE for DO white dwarfs model at** 100000 **K,** $\log g = 8$**, He/H=** 10^2**.**

shown, the Balmer lines are strongly modified in LTE atmospheres with nHe/nH = 10^5 or 10^4 and temperatures not much higher than 40000 K, this may be an artifact caused by the assumption of LTE. The influence of small traces of helium on the Balmer lines

vanishes for NLTE atmospheres. If LTE analysis of the hydrogen lines is to be performed it is recommended to use pure hydrogen models, even if it is likely that trace elements are present in the atmosphere, Napitwoski(1997).

Hubeny et al.(1999), computed two grids for DA white dwarfs with pure hydrogen atmosphere and metal rich DA white dwarfs. Figure (3.11), summarizes the results of the Balmer line analyses for all the stars in the sample for several model types pure hydrogen LTE, pure hydrogen non-LTE and high metalicity non-LTE with all heavy elements included. Two general features are immediately apparent. First, the effective temperature obtained with the heavy elements rich non-LTE models is systematically lower than for pure hydrogen LTE models. Second, although significant temperature differences are seen, there is little apparent effect on the gravity, Figure (3.12).

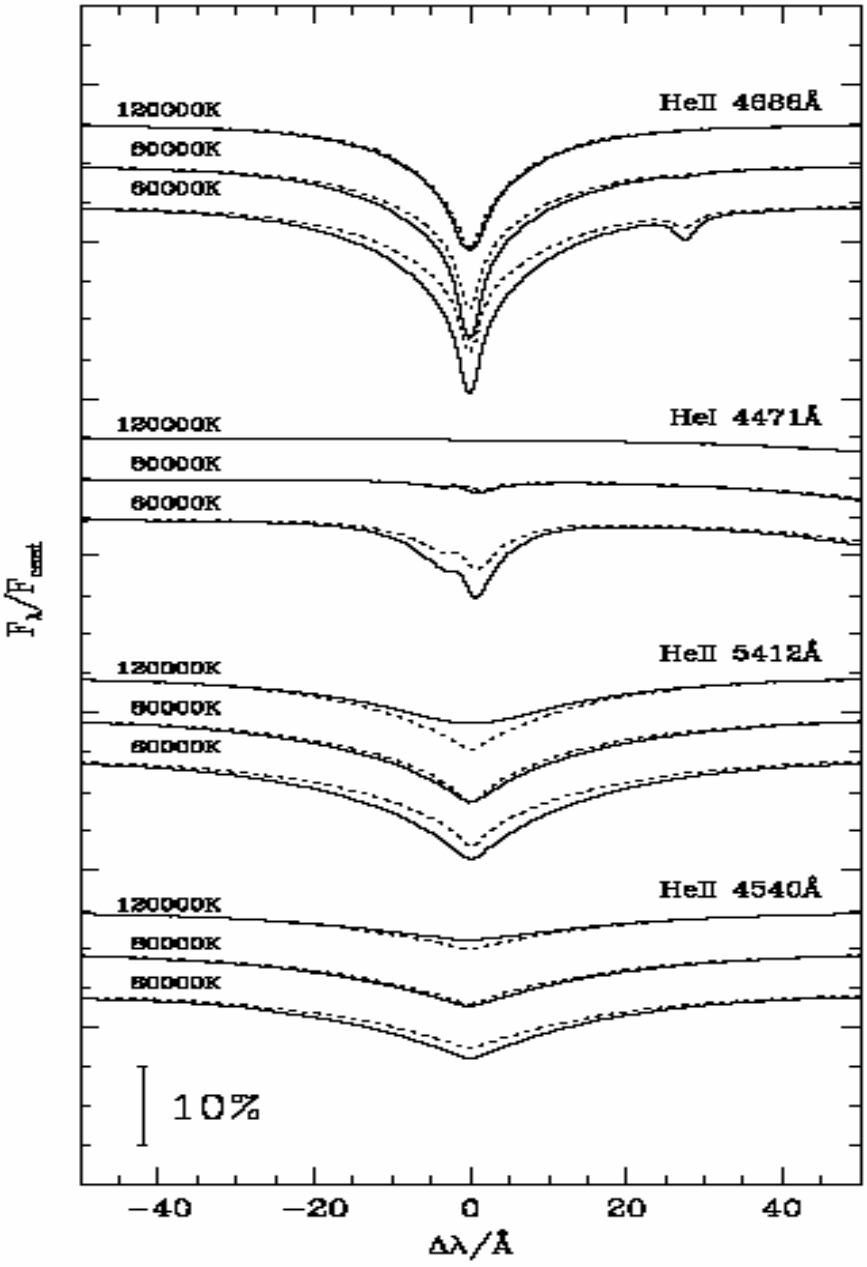

Figure 3.10: **Line profiles computed for DO model atmospheres at different temperatures (nHe/nH = 100, log g = 7.5). NLTE is drawn with solid lines, LTE with dashed lines. The profiles are convolved with a Gaussian of 2 ÅFWHM.**

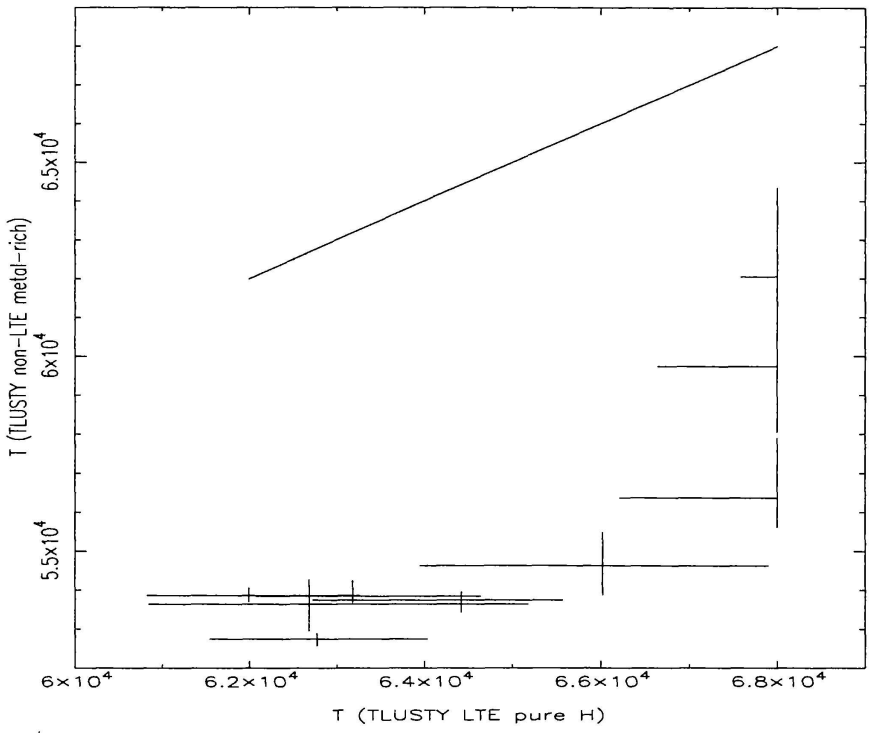

Figure 3.11: **Values of T_{eff} determined from Balmer line analyses using high metalicity non-LTE models versus the result from the pure hydrogen LTE studies.**

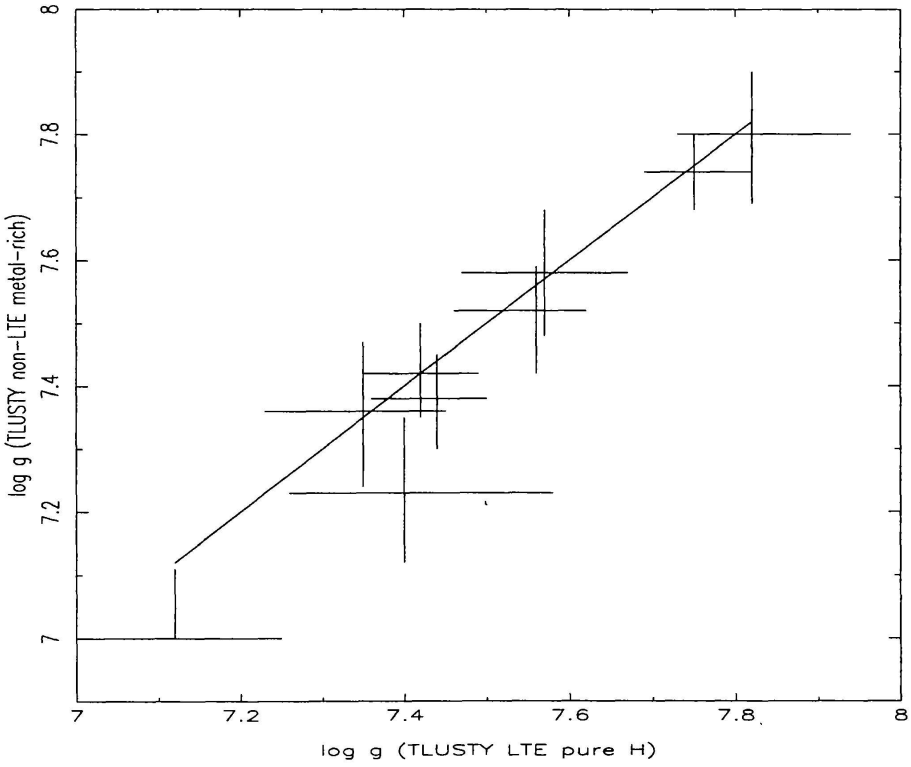

Figure 3.12: **Values of *logg* determined from Balmer line analyses using high metalicity non-LTE models versus the result from the pure hydrogen LTE studies.**

Chapter 4

Conclusion and Outlook

4.1 Introduction

Stellar atmospheres can be considered as laboratories of plasma physics, in which the atomic parameters can be tested. Also the mathematical methods developed in stellar atmospheres can be widely used in many other problems in astronomy (Mihalas, 1978).

In astrophysics, one of the importance of modelling stellar atmosphere is that it provides an adequate surface boundary condition for the computation of evolutionary stellar models. Besides, the atmosphere models are necessary to determine the emergent flux from the star, which is required to interpret the luminosities and colors of observed stellar spectra.

Since the pioneering work of Unsold in the 1930s and 40s (Unsold 1955) great progress has been made in the field of stellar atmosphere research. This has been driven by different activities. The first is the enormous progress in observational techniques. The quality of ground-based observations has increased dramatically thanks to the use of new detectors, e.g. CCDs. Data from space observatories in the X-ray, UV and IR allow us to probe different parts of a stellar atmosphere. The second action is the development of numerical methods to describe the atmosphere structure and radiative transfer. It has also become evident that several of the simplifying assumptions are not good enough. New developments in atomic physics made it possible to compute accurate energy levels, transition probabilities and line-broadening data.

4.2 Overview of the Present Theoretical Models

Model atmospheres can be classified as being of three general types: radiative equilibrium, general equilibrium, semi-empirical, and hydrodynamical.

- **Radiative equilibrium models** for which the temperature distribution is determined so that the outward radiative flux is constant with depth. Radiative equilibrium models assume that there are no sources of non-radiative heating, and are normally time-independent without mass flows. Except in special cases, the temperature decreases monotonically with decreasing depths. Examples are the deeper layers of stellar atmospheres (photospheres) that show no evidence of non-radiative heating effects.

- **General equilibrium models** are usually time-independent but include the effects of non-radiative energy flow due to thermal conduction, particle diffusion, and mass flows, and can include mechanical heating specified in some parametric way. Examples are the thin transition regions between neutral and ionized regions where a very steep temperature gradient results from strong resonance line cooling at the lower temperatures. See Fontenla, Avrett, & Loeser (2002).

- **Hydrodynamical models** simulate dynamical processes and use their properties to supply the mechanical heating necessary to account for an observed spectrum that shows emission in excess of that determined by radiative equilibrium. Such hydrodynamical models must assume some initial conditions to get the gas motions started, but then the model relies on internal wave motions to produce the mechanical heating. The aim in such calculations is to include all important physical processes and to match the given observations well enough to have confidence that the simulation is realistic. The time-dependent hydrodynamical models cannot be expected to lead to good agreement with observations if any important physical processes are not included or are not treated correctly. To the extent that the hydrodynamical models agree with observations they tell us more about the physical mechanisms at work than can be learned from the semi-empirical models, since the latter can indicate only the

general properties of the temperature and mechanical heating distributions yielding a given spectrum. In extreme cases the variations with time in hydrodynamical models can be very large, suggesting that time-averaged quantities in a corresponding time-independent semi-empirical model may not properly represent the physical conditions in the atmosphere. Examples are the dynamical solar atmospheric models of Carlsson & Stein (1997, 1999).

4.3 An Old-New Method: The Inversion Techniques

The stellar model atmospheres codes described in chapter 2 and chapter 3 are theoretical, as are almost all other models. However, the properties of the stellar atmospheres are encoded in the observed stellar spectra which at least in principle can be deciphered to yield the photospheric structure using inversion techniques, then the result is semi-empirical model atmosphere. This method has often been employed among solar physicists with the Holweger-Muller(1974) and the VAL-3C(Vernazza et al. 1981) solar models being the most well-known examples.

Semi-empirical models use a prescribed temperature distribution which is selected to obtain agreement between the spectrum calculated from the model and an observed spectrum. From such a model one can use the calculated departures from constant radiative flux to infer the corresponding mechanical heating distribution. Examples are stellar chromospheres that show emission due to an outward increase in temperature caused by the dissipation of mechanical energy in some form. See Vernazza, Avrett, & Loeser (1981) and Avrett (2002).

Surprisingly, such semi-empirical model atmospheres have rarely been used for stellar spectroscopy. It is believed that the time is now ripe for pursuing such modelling, in fact crucial in order to make optimum use of future satellite and ground-based telescope facilities.

Perhaps the biggest problem with using the above-mentioned theoretical model atmospheres for stellar abundance analyses is their computationally intensive nature. Although less sophisticated model atmospheres are less CPU-demanding, also standard abundance

analyses are time-consuming in terms of the work involved. To fully disentangle the formation and evolution of for example our own Galaxy would require a far more ambitious approach with much larger stellar samples(Freeman & Bland-Hawthorn 2002).

Fortunately this is now becoming feasible with new multi-object high-resolution spectrographs like FLAMES/VLT and the RAVE projects (Steinmetz et al. 2002) and the GAIA satellite(Perryman et al. 2001). The wealth of information these facilities will provide is truly astonishing, as is the magnitude of data needed to be analysed. Without an efficient automatic procedure to derive the inherent information in the spectra, these projects will not come to an optimal execution. **Semi-empirical model atmospheres represent one such promising possibility, provided the spectral resolving power is sufficient**.

Semi-empirical model atmospheres are obtained through an iterative procedure aimed at improving the overall agreement between the calculated and observed spectra. Since the temperature structure is modified in this way, the model does not in general fulfill flux constancy as in standard theoretical model atmospheres, nor is there any need to invoke uncertain and questionable recipes for convective energy transport, such as the mixing length theory, which can lead to grossly misleading results(e.g. Asplundet al. 1999; Asplund & Garciá Pérez2001). In fact, this allows at least in principle a possibility to gain insight to convection and non-standard energy transport, such as acoustic and magnetic heating. With the temperature determined from the observations, the gas pressure is normally fixed by the assumption of hydrostatic equilibrium while the electron pressure is the result of the ionization balance using the current estimate of the chemical composition. Thus knowledge of the surface gravity is necessary from for example parallaxes or photometry unless it can be obtained from satisfying the ionization balance of some key elements.

The main disadvantages with semi-empirical modelling comes with the numerical difficulties often associated with ill-posed inversion problems (e.g. ill-matrix) and the assumption of LTE normally made in the line formation calculations. The former can to a large extent be overcome by including a wide range of spectral lines with different line formation depths, ionization stages and excitation potentials. Of particular importance, at least for

late-type stars, is to include elements with both neutral and ionized lines and strong lines with pressure-damped wings. Although not yet utilized, hydrogen lines as well as various molecular lines have a great potential in this respect. The second major shortcoming can only be resolved by relaxing the assumption of LTE, which automatically makes the inversion procedure much more challenging and cumbersome. Very little work with the exception of the pioneering contribution by Soccas-Navarro et al. (1998) has been done on non-LTE inversion. It is, however, of absolute pivotal importance to include such effects, given the fact that LTE is often a poor assumption for the line formation process, leading otherwise to erroneous atmospheric structures and inferred conclusions.

Recent endeavours like the Opacity Project and Iron Project have come a long way in addressing the great needs for atomic data for non-LTE calculations. Although it would be advantageous to treat all elements in non-LTE for the inversions, as a first step it may be sufficient to do so for the most important elements for determining the actual atmospheric structure, such as Fe, Mg and Ca, while the line formation of other significant species for late-type stars like H and various molecules(e.g. CO) can likely be well approximated by LTE. Other trace elements which are unimportant for setting the atmospheric structure but whose abundance may be of interest can then be handled either in LTE or non-LTE after the initial inversion has converged. This procedure should restrict the computing time to just a few times a normal non-LTE calculation with a fixed 1D atmosphere.

Bibliography

[1] Allende Prieto, C.; Hubeny, I.; Lambert, D. 2003, Ap&J, 531, 1192

[2] Anderson, L. S. 1989, ApJ, 339, 558

[3] Anderson, L. S. 1989, Numerical Radiative Transfer, edited by Wolfgang Kalkofen. Cambridge: University Press, 1987., p.163

[4] Anderson, L. S. 1990, Properties of Hot Luminous Stars (ASP Conf. Ser.) 7 p 77

[5] Asplund, M., Nordlund, A., Trampedach, R., Stein, R.F. 1999, A&A, 346, L17

[6] Asplund, M., Garcia Perez, A.E. 2001, A&A, 372, 601

[7] Auer, L. H., & Mihalas, D. 1969, ApJ, 158, 641

[8] Auer, L. H. & Mihalas, D. 1972, Ap&JS, 24, 193

[9] Auer, L. H. 1987, in Numerical Radiative Transfer, ed. W. Kalkofen, Cambridge University Press, 101

[10] Bergeron P., Wesemael F., Beauchamp A., Wood M.A., Lamontagne R., Fontaine G., Liebert J. 1994, ApJ 432, 305

[11] Broyden, C. G. 1965, Math. Comp., 19, 577

[12] Carlsson, M. & Stein, R. F. 1997, LNP, 489, 159

[13] Carlsson, M. & Stein, R. F. 1999, AIPC, 471, 23

[14] Castor, J. I.; Abbott, D. C. & Klein, R. I. 1975, Ap&J, 195, 175

[15] Dreizler, S., &Werner, K. 1991, in Stellar Atmospheres: Beyond Classical Models, NATO ASI Series C, Vol. 341, ed. L. Crivellari, I. Hubeny & D.G. Hummer, (Dordrecht: Kluwer), 155

[16] Fontenla, J. M.; Avrett, E. H. & Loeser, R. 2002, Ap&J, 572, 636

[17] Freeman K.C., Bland-Hawthorn J. 2002, AR&AA, 40, 487

[18] Gabler, R.; Gabler, A.; Kudritzki, R. P.; Puls, J.& Pauldrach, A. 1989, A&A, 226, 162

[19] Hamann, W.-R., Koesterke, L., &Wessolowski, U. 1991, in Stellar Atmospheres: Beyond Classical Models, NATO ASI Series C, Vol. 341, ed. L. Crivellari, I. Hubeny & D.G. Hummer, (Dordrecht: Kluwer), 69

[20] Hauschildt, P. H., Allard, F., & Baron, E. 1999, ApJ, 512, 377

[21] Holweger, H., Muller, E.A. 1974, Solar Physics, 39, 19

[22] Hubeny, I. 1988, Comput. Phys. Commun., 52, 103

[23] Hubeny, I. 1992, Atmospheres of EarlyType Stars (Berlin: Springer) p 233

[24] Hubeny, I., & Lanz, T. 1992, A&A, 262, 501

[25] Hubeny, I. & Lanz, T. 1993, IAU Coll. 138 (ASP Conf. Ser.), 44, 98

[26] Hubeny, I., Hummer, D. G., & Lanz, T. 1994, A&A, 282, 157

[27] Hubeny, I., & Lanz, T. 1995, Ap&J, 439, 875

[28] Hubeny, I.; Barstow, M. A.; Lanz, T.; Holberg, J. B. 1999, ASPC, 169, 445

[29] Hügelmeyer, S.; Dreizler, S.; Werner, K.; Krezesinski, J.; Nitta, A. & Kleinman, S. 2005, A&A, 442, 309

[30] Hummer, D. G., & Mihalas, D. 1988, ApJ, 331, 794

[31] Husfeld, D.; Kudritzki, R. P.; Simon, K. P.; Clegg, R. E. S. 1984, A&A, 134, 139

[32] Kantorovich L. V. 1949, Trudy Mat. Inst. Steklova, XXVIII, 104

[33] Kubat, J. 1997, A&A, 324, 1020

[34] Kubt, J.; Korckov, D. 2004, IAUS, 224, 13

[35] Kudritzki, R. P. 1976, A&A, 52, 11

[36] Kurucz, R.L. 1993, CD-ROM 13

[37] Lanz, T. & Hubeny, I. 2003, Ap&J, 146, 71

[38] Lanz, T. & Hubeny, I. 2007, Ap&J, 169, 83

[39] Lucy, L. B. 1964, in First Harvard Smithsonian Conference on Stellar Atmospheres, Smithsonian Astrophysical Observatory Special Report No. 167, Cambridge, Massachusetts, 93

[40] Mihalas, D. 1972, NonLTE Model Atmospheres for B and O stars (NCARTN/STR), 76, 1

[41] Mihalas, D., & Hummer, D. G. 1973, ApJ, 179, 827

[42] Mihalas, D., Auer, L. H., & Heasley, J. N. 1975, NCAR Technical Note STR-104, (Boulder: National Center for Atmospheric Research)

[43] Mihalas, D.; Heasley, J. N. & Auer, L. H. 1975, STIN, 7630, 128

[44] Mihalas, D. 1978, Stellar Atmospheres, 2nd edition, (San Francisco: Freeman)

[45] Ng, K. C. 1974, J. Chem. Phys., 61, 2680

[46] Nouh, M. I. & Fouda, D. 2007, COSKA, 37, 189

[47] Olson, G. L., Auer, L. H., & Buchler, J. R. 1986, JQSRT, 35, 431

[48] Olson, G. L., & Kunasz, P. B. 1987, JQSRT, 38, 325

[49] Pauldrach, A.; Puls, J. & Kudritzki, R. P. 1986, A&A, 164, 86

[50] Pereira, T. 2009, Ph.D Thesis, The Australian National University

[51] Perryman M.A.C., de Boer K.S., Gilmore G., et al. 2001, A&A, 369, 339

[52] Rauch, T. & Werner, K. 1991, Stellar Atmospheres: Beyond Classical Models (NATO ASI Series C), 341, 165

[53] Rauch, T. 1993, A&A, 276, 171

[54] Rauch, T. 1997, A&A, 320, 237

[55] Sellmaier, F.; Puls, J.; Kudritzki, R. P.; Gabler, A.; Gabler, R.& Voels, S. A. 1993, A&A, 273, 533

[56] Scharmer, G. B., & Nordlund, A. 1982, Stockholm Observatory Report 19

[57] Schubert, L. K. 1970, Math. Comp., 24, 27

[58] Short, C. I. & Hauschildt, P. H. 2005, ApJ, 618, 926

[59] Short, C. I. & Hauschildt, P. H. 2009, ApJ, 691, 1634

[60] Soccas-Navarro H., Ruiz Cobo B., Trujillo Bueno J. 1998, Ap&J, 507, 470

[61] Steinmetz M., 2002, [astro-ph/0211417]

[62] Unsold, A., 1955, QB, 461, U55

[63] Vernazza J.E., Avrett E.H., Loeser R. 1981, Ap&JS, 45, 635

[64] Werner, K. 1986, A&A, 161, 177

[65] Werner, K. 1987, PhD Thesis, Universität Kiel

[66] Werner, K. 1996, A&A, 309, 861

View publication stats